Spring 5-31-2016

Preparation, ignition and combustion of reactive metal-sulfur nanocomposites

Ziyue Zhong
New Jersey Institute of Technology

Copyright Warning & Restrictions

The copyright law of the United States (Title 17, United States Code) governs the making of photocopies or other reproductions of copyrighted material.

Under certain conditions specified in the law, libraries and archives are authorized to furnish a photocopy or other reproduction. One of these specified conditions is that the photocopy or reproduction is not to be "used for any purpose other than private study, scholarship, or research." If a, user makes a request for, or later uses, a photocopy or reproduction for purposes in excess of "fair use" that user may be liable for copyright infringement,

This institution reserves the right to refuse to accept a copying order if, in its judgment, fulfillment of the order would involve violation of copyright law.

Please Note: The author retains the copyright while the New Jersey Institute of Technology reserves the right to distribute this thesis or dissertation

Printing note: If you do not wish to print this page, then select "Pages from: first page # to: last page #" on the print dialog screen

ABSTRACT

PREPARATION, IGNITION AND COMBUSTION OF REACTIVE METAL-SULFUR NANOCOMPOSITES

by
Ziyue Zhong

Mechanical milling is applied to synthesize reactive metal-sulfur nanocomposites. Specifically, magnesium-sulfur, aluminum-sulfur and zirconium-sulfur nanocomposite powders are prepared. Each powder particle contained homogeneously mixed sulfur and respective metal. These materials are expected to be stable in room air. They are also expected to release sulfur upon ignition; the released sulfur may serve as a biocidal agent. The ignition temperatures of the three prepared sulfur-bearing materials fall in a range of 750 – 1000 K. All prepared materials are successfully ignited in electrostatic discharge experiment as well as in a constant volume explosion experiment. The most sensitive material to spark ignition is magnesium-sulfur composite. In aerosolized combustion experiment, magnesium-sulfur exhibits the highest burning efficiency and highest rate of pressure rise. Materials with larger particle sizes appear to have longer ignition delays. Shorter burn times measured in the electrostatic discharge ignition test correlate with the greater rates of pressure rise obtained in the constant volume explosion test.

PREPARATION, IGNITION AND COMBUSTION OF REACTIVE METAL-SULFUR NANOCOMPOSITES

by
Ziyue Zhong

A Thesis
Submitted to the Faculty of
New Jersey Institute of Technology
in Partial Fulfillment of the Requirements for the Degree of
Master of Science in Chemical Engineering

Otto H. York Department of
Chemical, Biological and Pharmaceutical Engineering

May 2016

APPROVAL PAGE

PREPARATION, IGNITION AND COMBUSTION OF REACTIVE METAL-SULFUR NANOCOMPOSITES

Ziyue Zhong

Dr. Edward L. Dreizin, Thesis Advisor Professor of Chemical Engineering, NJIT	Date
Dr. Laurent Simon, Committee Member Associate Professor of Chemical Engineering, NJIT	Date
Dr. Mirko Schoenitz, Committee Member Associate Research Professor of Chemical Engineering, NJIT	Date

BIOGRAPHICAL SKETCH

Author: Ziyue Zhong

Degree: Master of Science

Date: May 2016

Undergraduate and Graduate Education:

- Master of Science in Chemical Engineering,
  New Jersey Institute of Technology, Newark, NJ, United State, 2016

- Bachelor of Science in Applied Chemistry,
  South China Agriculture University, Guang Zhou, P.R China, 2014

Major: Chemical Engineering

Publications:

Abraham, A., **Zhong, Z.**, Liu, R., Grinshpun, S.A., Yermakov, M., Indugula, R., Schoenitz, M., and Dreizin, E.L., Preparation, ignition and combustion of Mg·S reactive nanocomposites. *Combustion Science and Technology*, (**2016**). *Submitted.*

Wang, S., Abraham, A., **Zhong, Z.**, Schoenitz, M., and Dreizin, E.L., Ignition and Combustion of Boron-based Al·B·I_2 and Mg·B·I_2 composites. *Chemical Engineering Journal*, 293, pp.112-117 (**2016**).

谨以此论文献给我的父亲钟楚忠，我的母亲郑晓云，我的妹妹钟梓岚，钟若岚。

感谢你们一直以来的支持，鼓励，陪伴，包容。

This thesis is dedicated to my beloved father, mother and two of my sisters.

For their support, encouragement and unconditional love.

也谨以此论文感谢完成论文期间一直陪伴我的邱琬翔。

This thesis is dedicated to xiaoyu, who has been staying with me throughout the accomplishment of thesis.

ACKNOWLEDGMENT

First of all, I want to personally thank Prof. Edward L. Dreizin for granting me the opportunity to conduct research and to be a part of the Energetic Materials group in NJIT. As my instructor, his consistent guidance kept me on the right track when I felt lost in this project. It is his professional knowledge and kindness that support me to achieve the accomplishment of this thesis. Besides the research area, he also inspired me how to be a better man by showing his kindness and care to his students and colleagues, which will be a life time influence on me.

Special thanks to Prof. Mirko Schoenitz for his technical support. I appreciate his assistance in solving those experimental problems and all the insightful ideas he shared with me.

I also want to express my appreciation to Prof. Laurent Simon for serving as my thesis committee member and his valuable opinions on how to better improve the thesis.

Finally, I want to thank my fellow students in this group for all their help and advices. Especially my mentor Dr. Ani Abraham, his countless help and encouragement throughout this year make me feel that rather than as my mentor, he is also like a friend, who always took care of me.

TABLE OF CONTENTS

Chapter		Page
1	INTRODUCTION……..……...	1
2	EXPERIMENTS…….…….	3
	2.1 Material Synthesis……..	3
	2.2 Material Characterization……...	5
	2.3 Characterization of Ignition and Combustion…….....	5
3	RESULTS…….	10
	3.1 An Exploratory Study of Al·S Composite Materials…….....	10
	3.1.1 The Effect of Milling Conditions…….....	10
	3.1.2 The Effect of Chemical Composition……...	11
	3.2 An Exploratory Study of Zr·S Composite Materials…….....	16
	3.3 Comparison of Different Metal-Sulfur Composite Powders Prepared by Arrested Reactive Milling ……...	19
	3.3.1 Particle Shape, Size and Morphology ……..	19
	3.3.2 Phase Composition ……...	22
	3.3.3 Filament Ignition Experiment ……..	23
	3.3.4 Spark Ignition ……...	27
	3.3.5 Aerosol Combustion..……...	31
4	DISCUSSION..……...……...……...……...……...……...	34
5	CONCLUSION……	41

LIST OF TABLES

Table		Page
2.1	Milling Parameters Used for Preparation of Al·S Composites Discussed in Section 3.1……	4
2.2	Milling Parameters Used for Preparation of Zr·S Composites Discussed in Section 3.2…….....	4
3.1	Summary of ESD Results…….....	19
3.2	Atmospheric Boiling Points of Elements Used to Prepare Composite Powders…….....	27

LIST OF FIGURES

Figure		Page
2.1	Heated filament setup used to measure ignition temperatures of the prepared powders……	6
2.2	Schematic diagram of the ESD ignition experiment…….....	7
2.3	Brass sample holder used in ESD experiments with surface coated with residue produced after an ignition event…….....	8
2.4	Constant volume explosion apparatus used for experiments……....	9
3.1	Normalized pressure traces for Al·S composite powders ignited in CVE tests……....	11
3.2	XRD patterns of sample 5, 6 and 7……....	12
3.3	Characteristic emission traces of emission pulses produced by ESD initiated Al·S powder milled with different molar composition…….	13
3.4	Average temporal characteristics of emission pulses produced by ESD initiated Al·S powder milled with different molar composition…….	13
3.5	Examples of recorded pressure traces of ignited sample 5, 6 and 7 in ESD test…….....	14
3.6	Summary of maximum normalized pressure change and emission produced by ESD initiated Al·S powder milled with different molar composition……...	15
3.7	XRD patterns of sample III (drying milling) and sample IV (wet milling)…….…….....	16
3.8	Examples of emission and pressure traces of ignited Zr·S powder in ESD experiment……...	17
3.9	Average temporal characteristics of emission pulses produced by ESD initiated Zr·S powder milled with different milling conditions……..	18
3.10	Backscattered SEM images of as milled powders of sample A, B and C….....	21
3.11	Particle size distribution for as milled powders of sample A, B and C measured by the laser scattering with a Coulter particle analyzer…….	22
3.12	X-ray diffraction patterns of as milled powders of sample A, B, and C…….	23

LIST OF FIGURES
(Continued)

Figure **Page**

3.13 Sequences of images captured by high speed camera in the filament ignition experiment for each sample…… 25

3.14 Ignition temperatures of samples A, B, C as a function of the heating rate…… 26

3.15 Emission traces and pressure signals produced by ESD initiated powders of sample A, B and C……... 28

3.16 Average normalized pressure change and emission produced by ESD initiated powders of sample A, B and C…… 29

3.17 Average temporal characteristics of optical emission pulses produced by ESD initiated powders of samples A, B, and C…… 30

3.18 The peak emission of the each ignited sample powder in ESD test as a function of spark energy…… 30

3.19 Normalized pressure traces of ignited powders of sample A, B, and C measured in CVE test……... 31

3.20 Summary of CVE results…… 32

3.21 XRD patterns of CVE combustion products……... 33

4.1 The maximum rates of pressure rise measured in the CVE tests as a function of ignition temperatures……... 34

4.2 The maximum rates of pressure rise measured in the CVE tests as a function of the average particle size……... 35

4.3 Ignition delays measured in the ESD tests as a function of the ignition temperatures…… 36

4.4 Ignition delays measured in the ESD tests as a function of the average particle sizes……. 36

4.5 Maximum normalized pressure of each sample measured in ESD test as a function of ignition temperatures…… 37

4.6 Burn time of each sample measured in ESD test as a function of mean particle size……... 38

LIST OF FIGURES
(Continued)

Figure **Page**

4.7 Maximum rate of pressure rise measured in CVE test as a function of burn time measured in ESD test…….. 39

4.8 Maximum normalized pressure measured in CVE test as a function of both normalized pressure and absolute pressure measured in ESD test…… 40

CHAPTER 1

INTRODUCTION

Powders of such metals as Zr, Al, Mg, and Ti are used as fuels or fuel components in propellants, explosives, and pyrotechnics because of their higher energy density compared to traditional energetic materials like TNT, RDX, or HMX [1]. Another application of such metals is to combine them with a halogen, e.g., iodine, to create a biocidal composite to counter bioweapons. A cloud of lethal spores, virus or micro-organisms can be generated by a bio-attack and typically high temperature is not enough to completely inactivate all of them [2, 3]. Thus, when a combination of metal and halogen is added to the explosive charge, a high temperature zone can be generated, in which halogenated combustion products are dispersed. Such a high temperature, chemically active cloud may be able to effectively eliminate harmful agents. Halogen containing materials including $Al{\cdot}I_2$ [4, 5], $Al{\cdot}CHI_3$ [6], $Al{\cdot}B{\cdot}I_2$ [7], $Mg{\cdot}B{\cdot}I_2$ [8] and $Ag{\cdot}Br$ [9] have been investigated previously and proven to be antibacterial. Other than metal halogen composite, thermites employing biocidal components, like $Al+I_2O_5$ and $Al+Ag_2O$ [3] were also shown as capable of neutralizing spores effectively.

Recently, sulfur has been considered as another candidate to counter bioweapons for its ability to produce gaseous bactericidal sulfur oxides [10]. In addition, sulfur is moisture and air stable and reacts exothermically with metals such as Mg, Zr, Mn, Fe. The adiabatic flame temperature of reaction between some metals such as Ca and Sr can be as high as 5000 K under specific circumstance [11]. The dual benefit of being antimicrobial and high energy releasing make a composite material combining metal and sulfur an

intriguing candidate for the present investigation. In this study, metastable nanocomposite were prepared by Arrested Reactive Milling, which has been extensively applied to synthesize reactive materials [12-14] as a versatile, scalable and inexpensive technique.

A method is presented for preparation of composite materials containing a reactive metal and sulfur mixed on the scale of less than 1 μm. The goal of this study is to expand the range of novel reactive materials, capable of high energy release and generation of biocidal combustion products. The main body of this report is separated into three parts:

(1) Investigation of Al·S composites;

(2) Investigation of Zr·S composites;

(3) Side by side comparison of three sulfur-bearing reactive materials: Mg·S, Al·S, Zr·S.

In the material investigation sections, the optimizing of milling condition and different attempt of varying the composition will be discussed. In the third section, all three materials are synthesized by Arrested Reactive Milling in an identical procedure to compare their ignition dynamics and combustion properties. The focus of this study is to prepare testable sulfur-bearing materials in a systematic fashion. For consistency, in the third part of this study, all prepared compositions contained 50% weight fraction of metal plus 50% weight fraction of sulfur. Future work may address compositions with varied metal to sulfur ratios, which may be optimized depending on a specific application.

CHAPTER 2

EXPERIMENTS

2.1 Materials Synthesis

Starting materials are elemental powders of magnesium, -325 mesh, 99.8% pure, purchased from Alfa Aesar; elemental powder of aluminum, -325 mesh, 99.5% pure, purchased from Atlantic Equipment Engineers; zirconium, 2-3 μm, 95% pure, purchased from Alfa Aesar; sulfur, -100 mesh, reagent grade, purchased from Sigma-Aldrich. A shaker mill (SPEX Certiprep, 8000 series) with two 50-mL flat-ended zirconia vials, equipped with two auxiliary air-jets for vial cooling was used for mechanical milling at room temperature. In most runs, 5mL of hexane was added into each vial as a Process Control Agent (PCA) to prevent mechanically triggered reactions during milling and minimize powder caking. Starting powders and weighed steel balls were loaded initially in each vial and sealed inside an argon-filled glovebox to secure a chemically stable environment. The Ball to the Powder mass Ratio (BPR) determines the mass of steel balls in respect to the powder load. The powder load was kept constant at 5 g in these experiments. The BPR, ball size and milling time were varied to alter the milling intensity. The goal was to synthesize a reactive composite material, with as fine mixing between components as possible, but with minimized chemical reaction; i.e., formation of metal sulfides was not desirable. Previous efforts aimed to synthesize Mg·S nanocomposite powders [15] served as a starting point for this work. In this study, the material investigation of Al·S was conducted by modifying both material composition and milling conditions, as listed in Table 2.1. Some samples reacted during milling, producing aluminum sulfide. These samples were discarded. For

Zr·S, the effects of PCA, BPR and ball size were also explored with details listed in Table 2.2.

In the comparison section, separate batches of composite materials of Mg·S, Al·S and Zr·S were milled in 5 ml of hexane for 60 minutes with 50 grams of 10-mm steel balls. Each powder load contained 2.5 grams of metal and 2.5 grams of sulfur. Samples A, B and C represented Mg·S, Al·S and Zr·S, respectively.

Table 2.1 Milling Parameters Used for Preparation of Al·S Composites Discussed in Section 3.1

Sample ID	Ball Size(mm)	Milling Time(min)	PCA (5mL hexane)	Al : S mole ratio	Reacted during milling
1	10	75	No	2 : 3	No
2	10	90		2 : 3	Yes
3	5	75	Yes	2 : 3	No
4	10	75		2 : 3	No
5	10	90		2 : 3	No
6	10	90		2 : 1.5	No
7	10	90		2 : 0.75	No

Note: BPR=10 for all samples.

Table 2.2 Milling Parameters Used for Preparation of Zr·S Composites Discussed in Section 3.2

Sample ID	BPR	Ball Size(mm)	PCA (5mL Hexane)
I	5	5	No
II	5	5	Yes
III	10	10	No
IV	10	10	yes

Note: All samples were milled for 60 minutes, no reaction during milling occurred.

2.2 Material Characterization

A LEO 1530 Field Emission scanning electron microscope (SEM) was used to investigate the mixing scale as well as the morphologies of the sample. Imaging was mostly using backscattered electrons to obtain the phase contrast between components. X-ray diffraction (XRD) was performed using a PANalytical Empyrean diffractometer to analyze the phase compositions of the as milled powders. In addition, combustion products collected from constant volume explosion experiments were studied. The diffractometer was operated at 45 kV and 40 mA using unfiltered Cu K_α radiation (λ = 1.5438 Å).

2.3 Characterization of Ignition, Combustion

Ignition of the prepared powders was characterized in air using a heated filament experiment, which was described extensively elsewhere [16, 17]. Schematically, the experimental setup is shown in Figure 2.1. A 1-cm long thin coating of hexane slurry of the powder was coated on a 4.5-cm long, 0.5-mm diameter nickel-chromium alloy heating wire. A DC current was applied to heat the coated wire. The experiments were operated at different heating rates in the range of 2000 – 20000 K/s, achieved by an adjustable applied voltage and resistor connected in series with the wire. A high-speed infrared pyrometer (DP1581 by Omega Engineering, Inc.) was used to measure the temperature of the filament focused on an uncoated filament surface adjacent to the part of coating. The ignition event of the powder coating was visualized using a high speed video camera (MotionPro 500 by Redlake), operated at 500 fps. Before the ignition, the coating surface was darker than that of the heated filament. The time when the powder became brighter than the heated filament was considered as ignition instant.

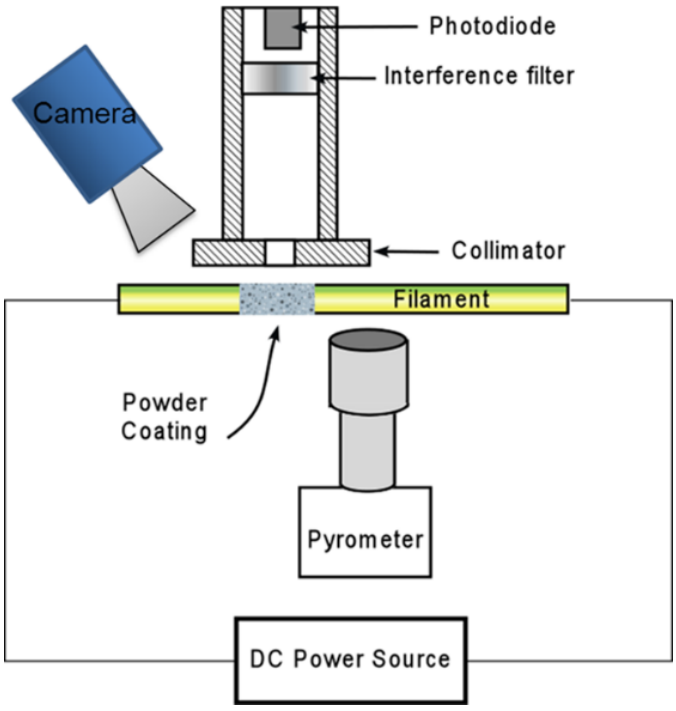

Figure 2.1 Heated filament setup used to measure ignition temperatures of the prepared powders.

Source: Shasha Zhang, Mirko Schoenitz and Edward L. Dreizin "Oxidation, Ignition and Combustion of Al-Hydrocarbon Composite Reactive Powders" New Jersey Institute of Technology, *International Journal of Energetic Materials and Chemical Propulsion*, 11 (2012) 353–373.

In an electro electro-static discharge (ESD) experiment, shown schematically in Figure 2.2, prepared powder was loaded in a 0.5-mm deep, 6-mm diameter cavity of a grounded, custom-made polished brass sample holder, which was placed in the center of a sealed chamber with a volume of 624 cm^3. The excess powder was scraped away by a razor blade to make an even layer thickness. The loaded sample holder was grounded. A high-voltage pin electrode was placed ~ 0.2 mm above the surface of the powder layer. A selected capacitor in a range from 250 to 2000 pF was initially charged to a voltage in a range of 3 – 12 kV. The capacitor was then discharged through the pin electrode and the powder sample. All tests were conducted in ambient air under room temperature. The

optical emission of ignited powder filtered at λ = 568 nm was measured by a photomultiplier tube (PMT), which was placed 15 cm away from the sample. The experimental chamber was equipped with a model 482A21 dynamic pressure transducer by Piezoelectronics to record the pressure change as a function of time. A more detailed description of the experimental procedure is available elsewhere [18, 19].

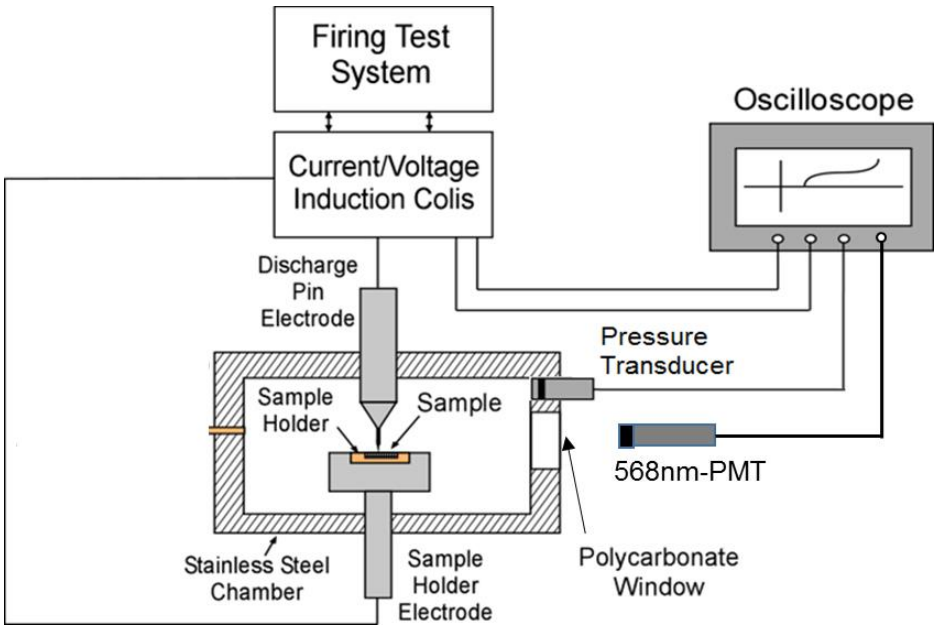

Figure 2.2 Schematic diagram of the ESD ignition experiment.

Source: Rayon A. Williams, Jaymin V. Patel and Edward L. Dreizin "Ignition of Fully Dense Nanocomposite Thermite Powders by an Electric Spark" New Jersey Institute of Technology, *Journal of Propulsion and Power*, 30 (2014) 765-774.

For the recorded optical emission pulses, five temporal characteristics were defined: the onset (t_{-10}) was defined as the time from the ESD ignition pulse to 10% of the emission peak height; the peak width was taken at half of the emission maximum, from t_{-50} to $t_{+50;}$ the peak position (t_{100}) was defined at the time the signal reached its maximum value; and the overall burn time (t_{+10}) was identified when the emission signal decreased to 10% of its peak value. Both measured emission and pressure traces were normalized by the weight of

powder ejected after the spark, which was calculated by subtracting the weight of the sample holder and residue (see Figure 2.3) from the initial weight of the powder-loaded sample holder.

Figure 2.3 Brass sample holder used in ESD experiments with surface coated with residue produced after an ignition event.

A larger scale combustion event was produced and characterized in a constant volume explosion (CVE) experiment. Schematic diagram of the apparatus is shown in Figure 2.4. Additional information regarding the experiment procedure can be found elsewhere [14, 20]. A 9.2 liters spherical explosion vessel was used. Initially, the powder was loaded in a pipe elbow under the vessel; a dispersion nozzle was mounted above the powder charge. Typically, 4.65 g of powder was loaded for each experiment. The reservoir was filled with air at a high pressure. The vessel was evacuated and then the powder was aerosolized by a blast of air from the reservoir controlled by a solenoid valve and passing through the pipe elbow containing the powder charge. The pressure in the vessel increased to 1 atmosphere after the air blast; this pressure was considered the starting value, P_0. After a 0.3-s delay necessary to minimize the turbulence, the combustion was initiated by a custom-made thermite igniter placed at the center of the vessel. The igniter was made of 0.1 g of Al/Fe_2O_3 thermite with a 4:1 Al : Fe_2O_3 mole ratio, loaded in a 5-cm diameter, 3.5-cm height steel tube. A 3-cm long tungsten wire was threaded through the thermite powder and was electrically heated to ignite the thermite. The pressure inside the vessel

was measured by a PX2AN1XX500PSAAX pressure transducer by Honeywell as a function of time. The energy released in the combustion event was quantified by the maximum normalized pressure: P_{max}/P_0; the rate of combustion was quantified by the maximum rate of pressure rise: $[d(P/P_0)/dt]_{max}$. The combustion products were collected and analyzed by the XRD.

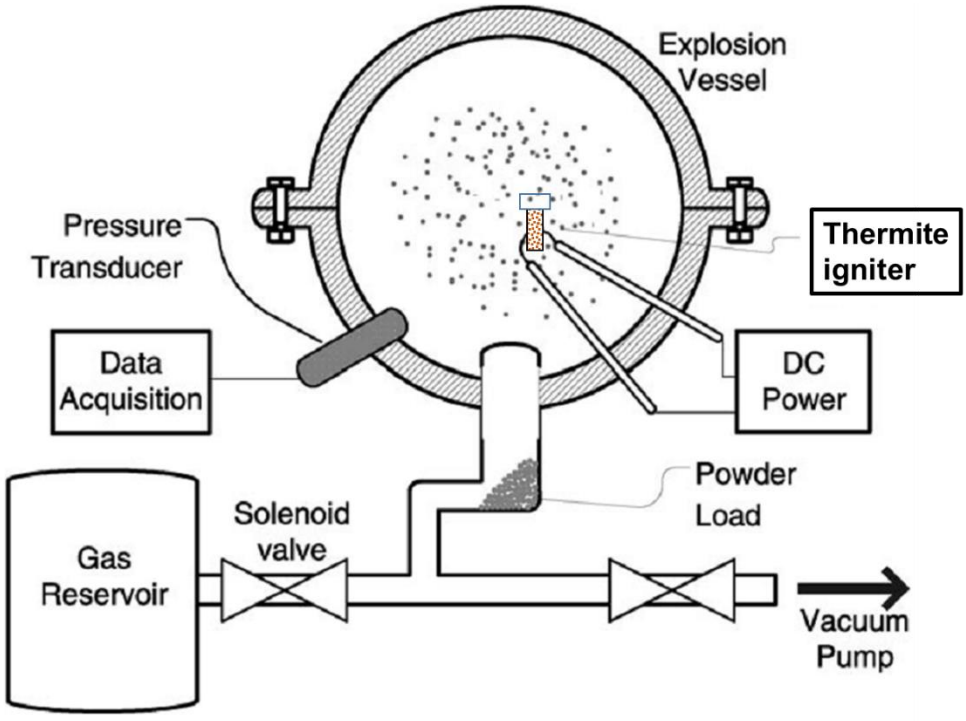

Figure 2.4 Constant volume explosion apparatus used for experiments.

Source: Demitrios Stamatis, Xianjin Jiang, Ervin Beloni and Edward L. Dreizin "Aluminum Burn Rate Modifiers Based on Reactive Nanocomposite Powders" New Jersey Institute of Technology, *Propellants, Explosives, Pyrotechnics*, 35 (2010) 260–267.

CHAPTER 3

RESULTS

3.1 An Exploratory Study of Al·S Composite Materials

The effect of milling conditions and Al to sulfur molar ratio will be discussed in this section. Initially, samples prepared with different milling conditions were characterized and compared to one another using the CVE experiment. Because the CVE experiment requires substantial amount of powder, experiments relying on ESD ignition were later performed to compare combustion of powders with different compositions. In the latter case, a much smaller amount of material was used and ignition was easier to achieve.

3.1.1 The Effect of Milling Conditions

In dry mechanical milling, samples milled with 5-mm balls produced hard chunks while samples milled with 10-mm balls produced fine powder without chunks; powder reacted at 90 minutes when 10-mm balls were used at BPR=10. In wet mechanical milling, chunks were not produced. Figure 3.1 presents pressure traces recorded in a CVE experiment for samples milled using different process parameters. All samples had the same composition; none of the tested samples reacted during milling.

In Figure 3.1, time zero corresponds to the initiation of the thermite ignitor. Sample numbers listed in the legend are referring to Table 2.1. Sample 5 prepared using a longer milling time produced the highest pressure, while the difference in pressure among other samples tested was negligible. It is observed that sample 3, prepared using smaller, 5-mm diameter balls, ignited faster than other materials.

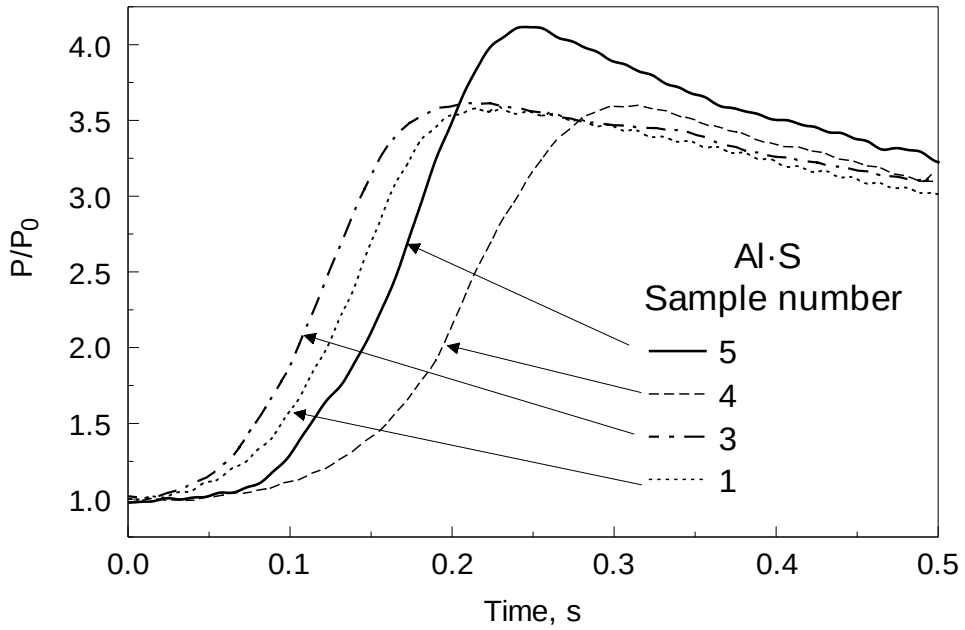

Figure 3.1 Normalized pressure traces for Al·S composite powders ignited in CVE tests.

Note: Samples 3, 4, 5 were prepared using wet milling, sample 1 was prepared by dry milling. Refer to Table 2.1 for further details.

3.1.2 The Effect of Chemical Composition

XRD patterns of the prepared powders (samples 5, 6 and 7, cf. Table 2.1) are shown in Figure 3.2. Only apparent crystalline Al peak and sulfur peak were detected, indicating no aluminum sulfide was formed after milling. The phase compositions of samples milled with different Al concentrations all show peaks of Al and S only. Therefore, prepared powders are composites comprising elemental Al and S, rather than sulfides.

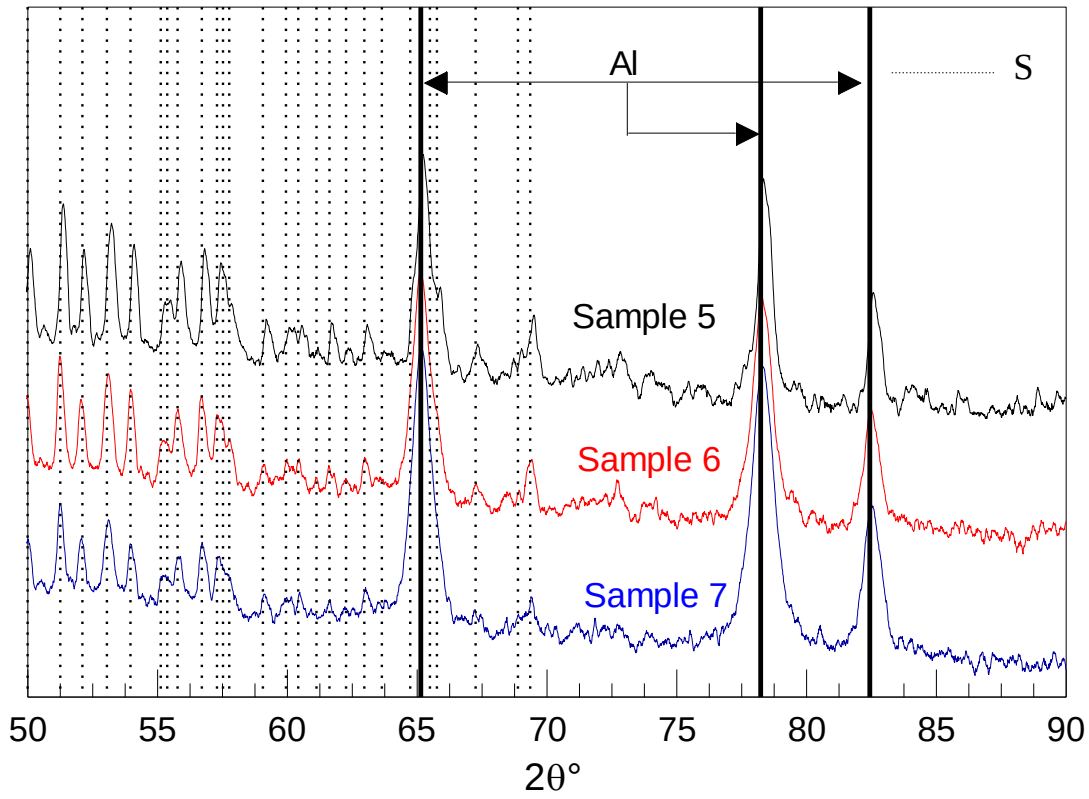

Figure 3.2 XRD patterns of sample 5, 6 and 7.

Note: Y axis are shifted with arbitrary unites.

In ESD tests, a 2000-pF capacitor charged to 12 kV was used to ignite sample powders. Examples of the emission traces measured in ESD test are shown in Figure 3.3. The overall pulse duration is close to 100-ms for all materials. Characteristic times (see Section 2.3) for the recorded emission pulses were measured and are summarized for all samples in Figure 3.4. Each characteristic time is presented as an average value with error bars showing the standard deviation from repeated runs. The shortest ignition delay was observed for sample 5 with the stoichiometric composition. For samples with greater aluminum concentrations, the ignition delays became progressively longer. However, the strongest emission intensity was observed for sample 6.

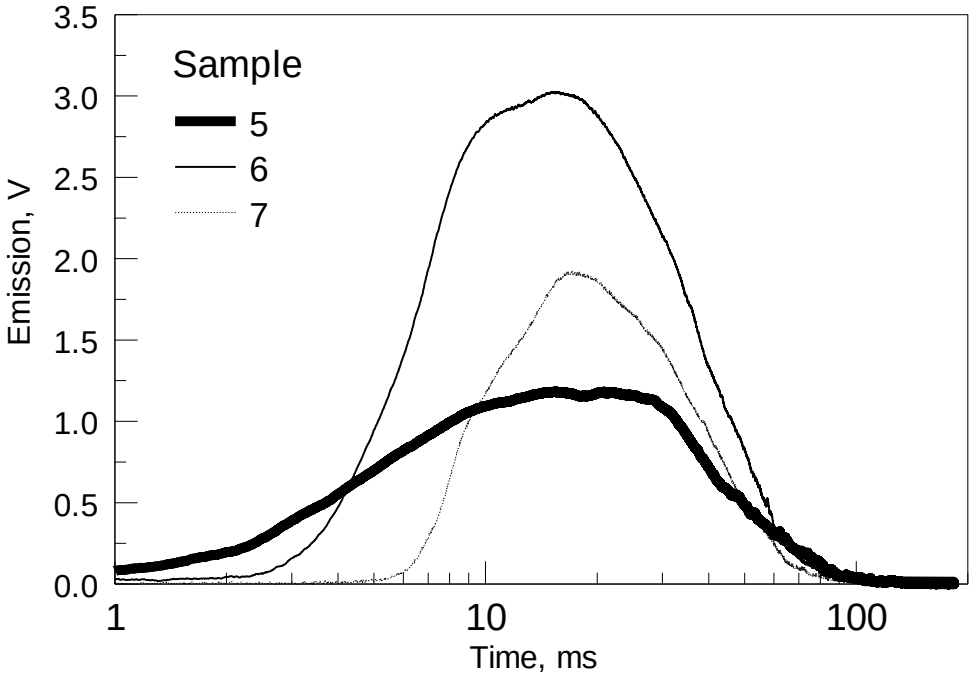

Figure 3.3 Characteristic emission traces of emission pulses produced by ESD initiated Al·S powder milled with different molar composition.

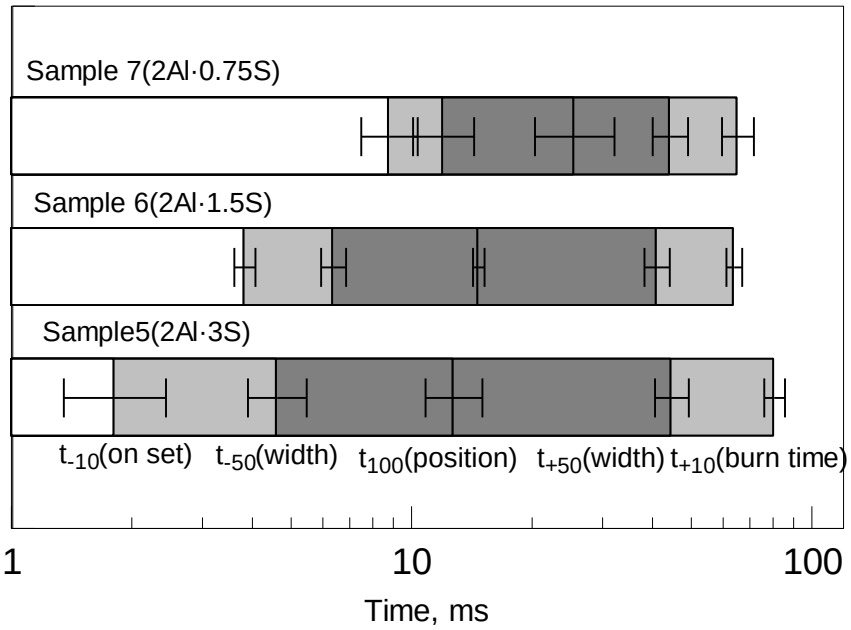

Figure 3.4 Average temporal characteristics of emission pulses produced by ESD initiated Al·S powder milled with different molar composition.

Examples of the recorded pressure traces are presented in Figure 3.5. The pressures start increasing later and the pressure peaks shift to longer times for samples with greater concentrations of aluminum. The delayed ignition for aluminum-rich samples implied by the pressure traces is consistent with the optical emission measurements shown in Figure 3.4. The absolute pressures observed for samples 5 and 6 are substantially higher than for sample 7.

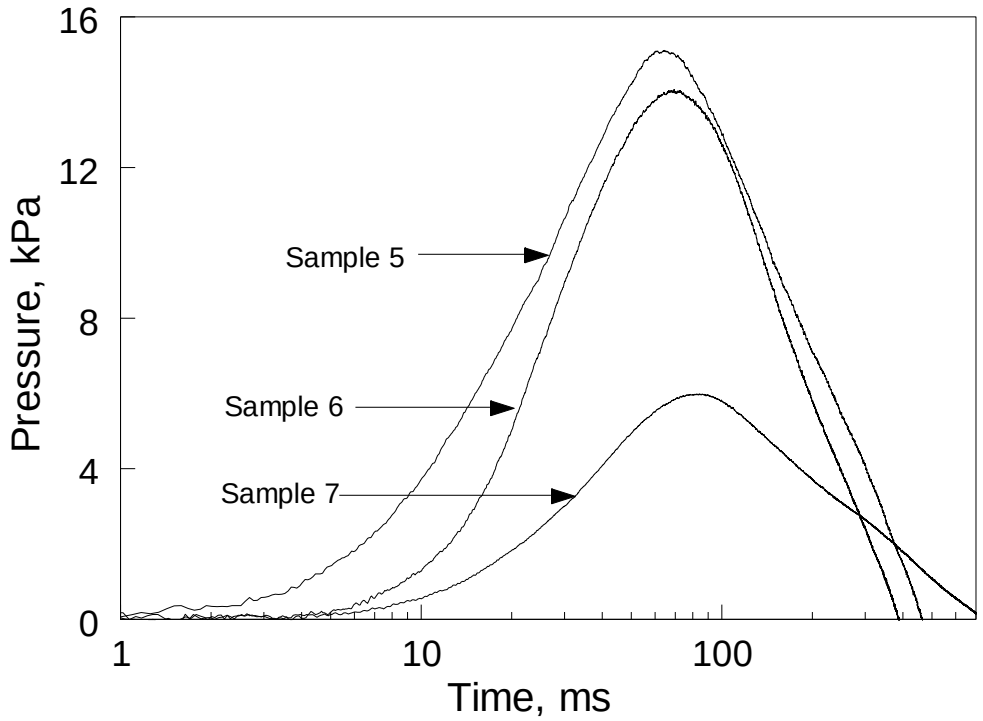

Figure 3.5 Examples of recorded pressure traces of ignited sample 5, 6 and 7 in ESD test.

For consistent comparisons of different runs to one another, the pressure change and peak emission were normalized by the mass of powder ejected from the sample holder. Shaded bars in Figure 3.6 show such normalized peak pressure values. They are compared, for each composition, with respective pressures calculated using NASA CEA code [21].

The calculations were performed for the constant volume configuration. Calculated maximum pressures are shown by the open bars. A ratio of the experimental to calculated maximum pressure is used as an indicator of combustion efficiency. Both maximum pressure and combustion efficiency are similar to each other for samples 5 and 6. However, combustion is much less efficient and results in a lower maximum pressure for the most aluminum rich sample 7. For comparison, normalized optical emission is also shown in Figure 3.6. It is highest for sample 6, for which the absolute normalized pressure is also slightly higher than for other materials. Thus, its composition with the Al to S mole ratio of 2:1.5 is most attractive.

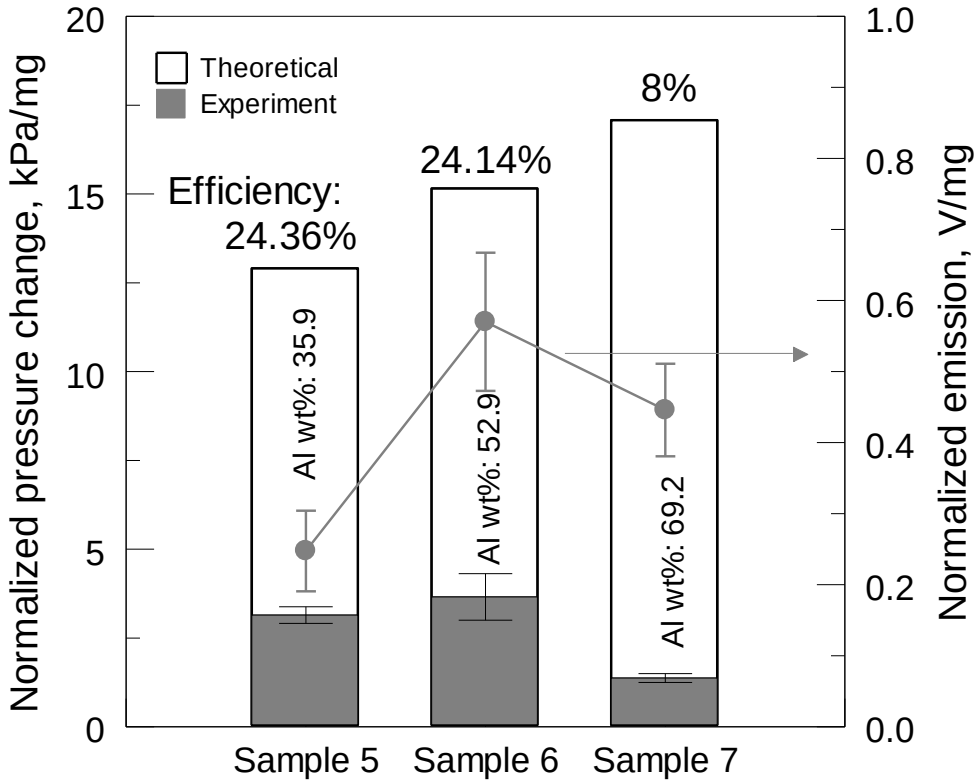

Figure 3.6 Summary of maximum normalized pressure change and emission produced by ESD initiated Al·S powder milled with different molar composition.

Note: Theoretic reference of equilibrium normalized pressure calculated by NASA CEA code are presented to estimate the efficiency of combustion.

3.2 An Exploratory Study of Zr·S Composite Materials

Milled powder of sample I was significantly caked; it contained hard agglomerates, which could not be easily broken apart. Thus, this sample is not used for further study. For samples II, III, and IV, agglomerated chunks were broken apart to recover fine powder. Results of XRD analyses for samples III and IV are shown in Figure 3.7. Only peaks of crystalline Zr are apparent in the pattern for dry-milled sample III. For the wet-milled sample IV, peaks of both Zr and S were detected.

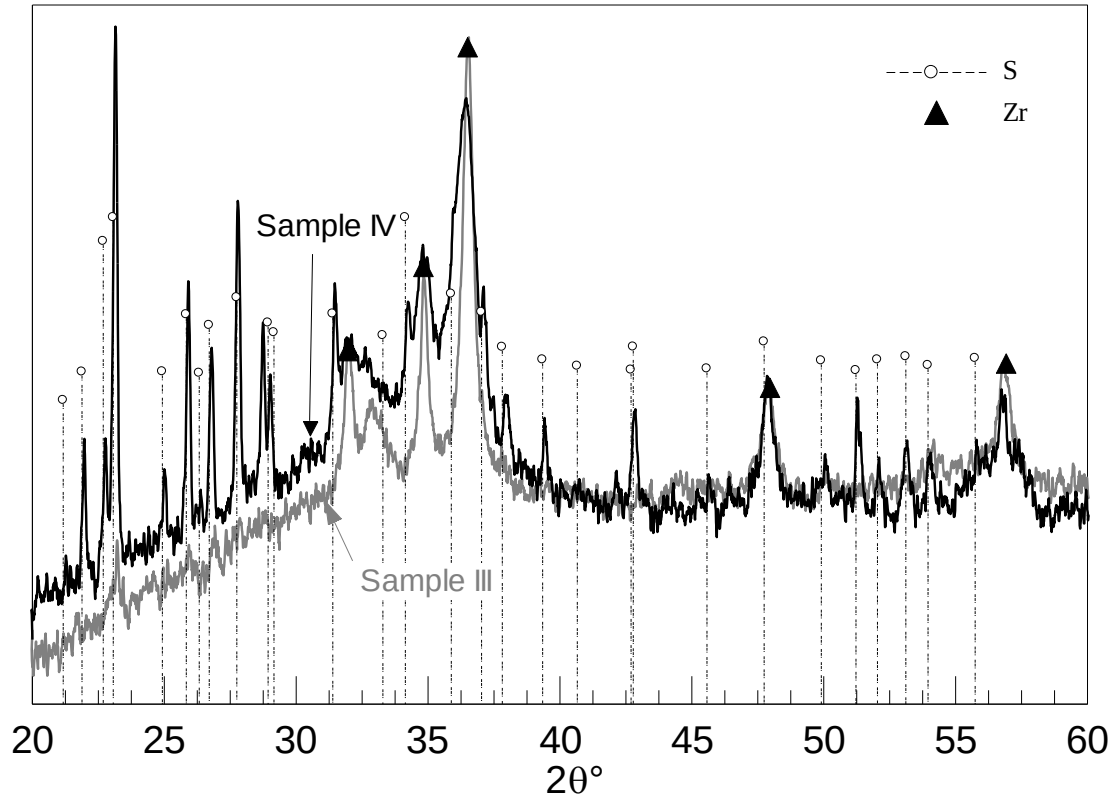

Figure 3.7 XRD patterns of sample III (drying milling) and sample IV (wet milling).

Emission and pressure traces recorded for different samples ignited by ESD are shown in Figure 3.8. A 2000-pF capacitor charged to 12 kV was selected to ignite sample powders. Details for the sample preparation are given in Table 2.2. Qualitatively, the traces

are similar for all materials. Emission traces begin immediately following the spark, although the peak emission is observed around 10 ms. The pressure increase begins after more than 1-ms delay. The peak of the pressure pulse roughly coincides with the end of the emission pulse, suggesting that the combustion duration can be reasonably determined from the duration of the entire emission pulse. The emission pulse appears to include two parts, which are most clearly separated for sample III, for which there are two distinct peaks are observed. The earlier peak was caused by the ignition of single particles (prompt ignition) directly heated by the spark. The delayed portion of the emission peak is caused by combustion of the aerosolized cloud.

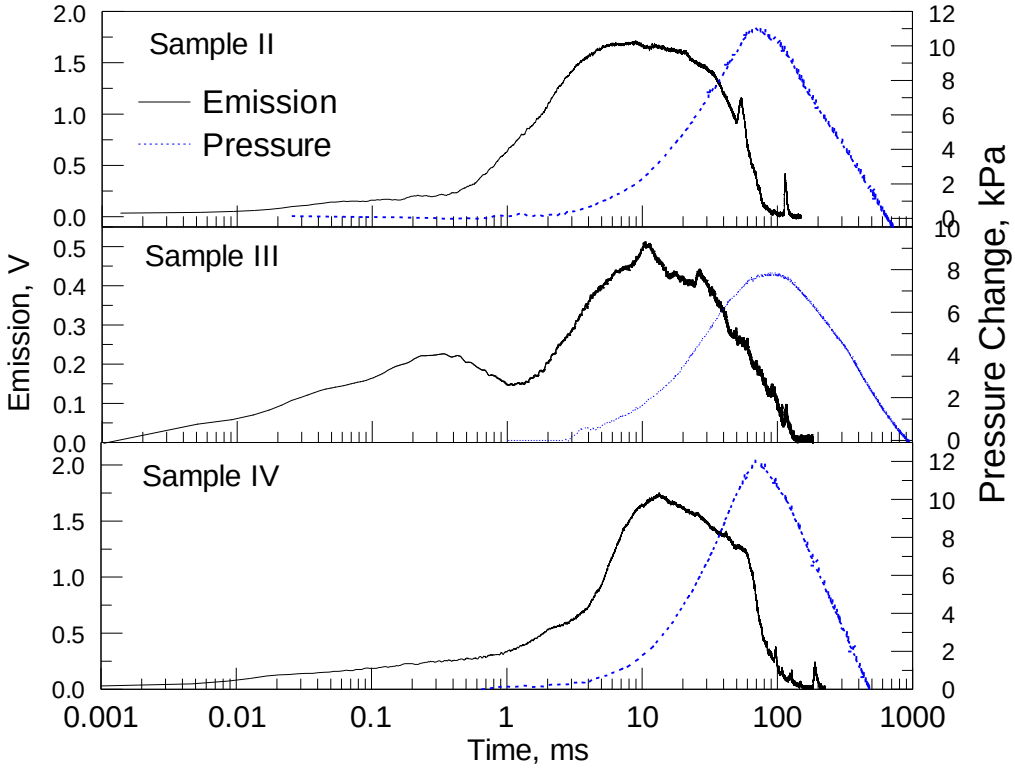

Figure 3.8 Examples of emission and pressure traces of ignited Zr·S powder in ESD experiment.

Temporal characteristics of the recorded emission pulses are shown in Figure 3.9. It appears that the dry-milled samples had shorter ignition delays for individual particles struck by the spark. However, they also had the longest delay until the emission peak produced by the burning particle cloud. The results shown in Figure 3.8 do not account for the amount of powder ejected from the sample holder. The measurements of the mass of ejected powder are taken into account in the data shown in Table 3.1.

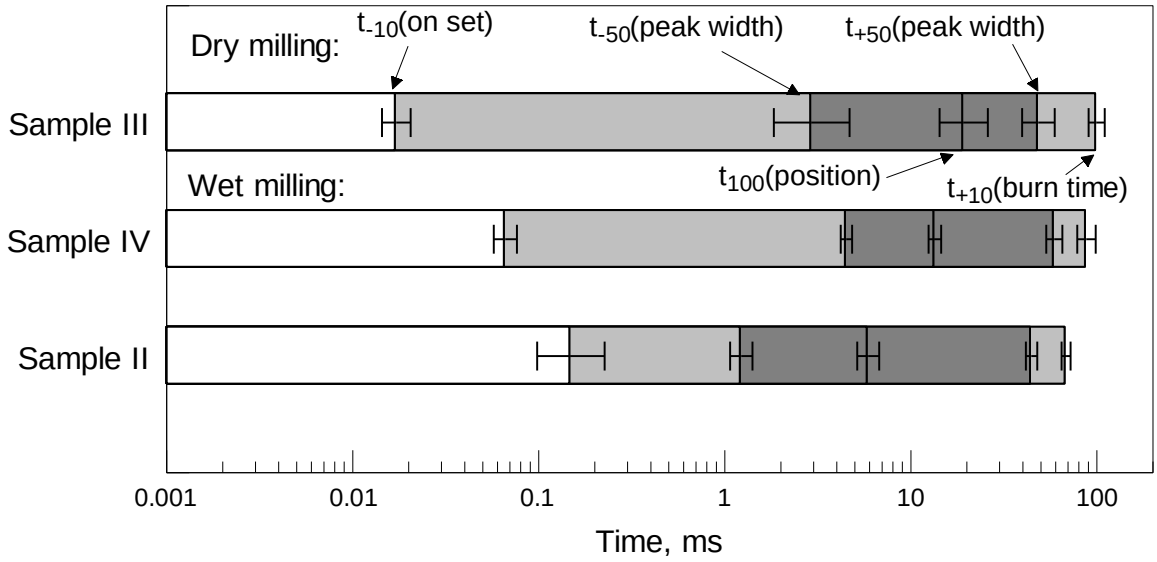

Figure 3.9 Average temporal characteristics of emission pulses produced by ESD initiated Zr·S powder milled with different milling conditions.

Theoretical pressures for all experiments were obtained using a thermodynamics equilibrium code CEA by NASA. A constant volume calculation was performed, considering the mass of the powder charge and volume of the experimental chamber. Efficiency is evaluated as the ratio of the measured to theoretical pressure rise. Efficiencies are expected to be low, considering a large volume of the chamber, and thus substantial heat losses during the experiment, which are neglected in the calculation. The ejected mass was much greater for the dry-milled sample III, compared to the wet-milled samples II and

IV. However, the measured amplitudes of the optical emission pulses and pressures were lower for this sample, resulting in very low values of normalized emission and pressure. Thus, although readily ejected and quickly ignited by the spark, dry milled material failed to burn as completely as the powders prepared by wet milling.

Table 3.1 Summary of ESD results

Sample ID	Weight loss(mg)	Normalized Emission (V/mg)	Normalized ΔP(kPa/mg)	Theoretical ΔP(kPa/mg)	Efficiency (%)
II	4.47 ± 0.50	0.40 ± 0.05	2.50 ± 0.30	8.30	30.1
III	11.8 ± 5.01	0.039 ± 0.018	0.48 ± 0.18	7.99	6.1
IV	4.60 ± 0.78	0.36 ± 0.04	2.19 ± 0.03	8.33	26.3

3.3 Comparison of Different Metal-Sulfur Composite Powders Prepared by Arrested Reactive Milling

Based on previous study, three composite powders including Mg·S, Al·S and Zr·S were synthesized in a consistent manner as described in Section 2.1. These materials were compared to one another in this part of the thesis.

3.3.1 Particle Shape, Size and Morphology

SEM images of samples A (Mg·S), B (Al·S), and C (Zr·S) are shown in Figure 3.10. The images were produced by backscattered electrons, which are sensitive to different atomic weight of elements. Thus, sulfur will appear as a brighter element in samples A, B. In sample C, zirconium will appear brighter than sulfur, however.

Sample A contains Mg flakes coated with fine spherical sulfur particles on the surface; it is possible that sulfur is also embedded in the volume of Mg flakes. This material

also includes unattached fine particles of Mg and sulfur. The range of particle sizes appears to be broader than for other samples.

For sample B, equiaxial particles consist of agglomerated Al flakes with sulfur captured in between. Similar to sample A, it is possible that sulfur is embedded in the volume of Al flakes. Particles appear to be coarser than for sample A.

Sample C appears to contain mostly crystalline sulfur particles coated by fine Zr particles. It is unlikely that zirconium is embedded in the volume of sulfur crystals. A longer milling time might be needed to produce a better homogenized composite material.

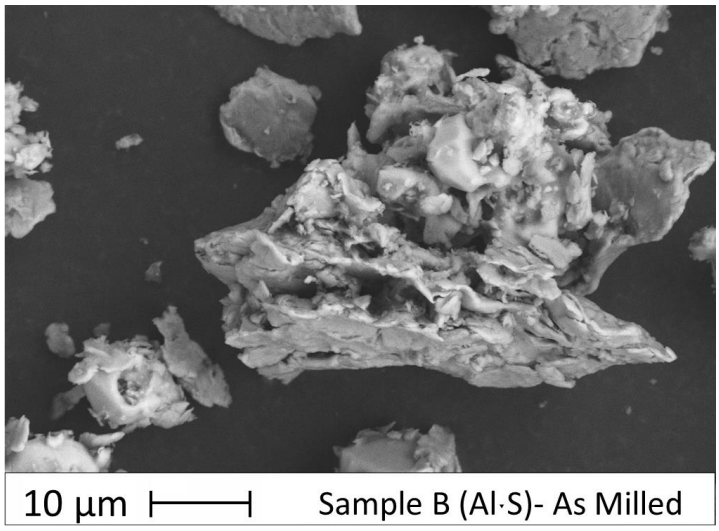

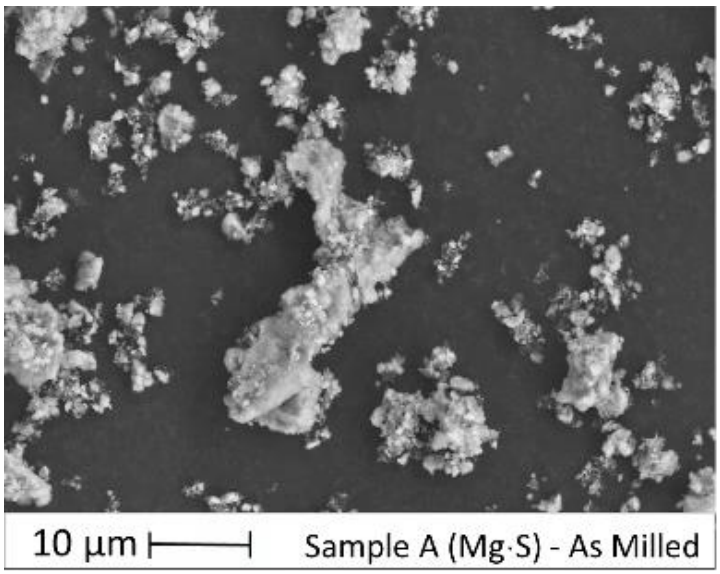

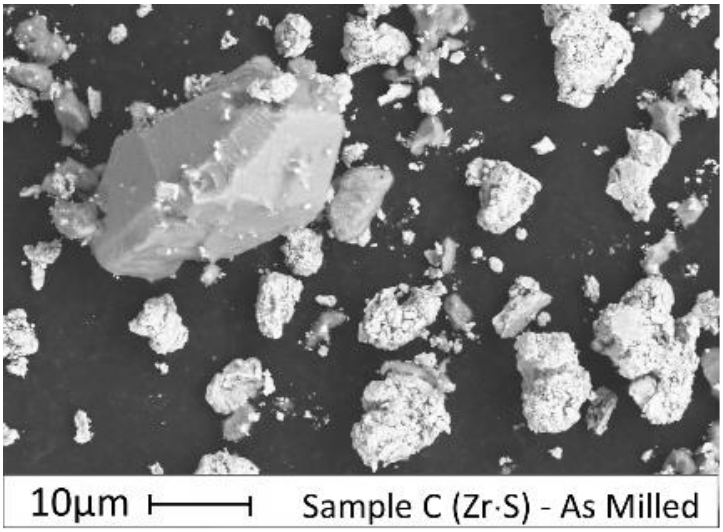

Figure 3.10 Backscattered SEM images of as milled powders of sample A, B and C.

Particle size distributions of each sample obtained using Coulter particle analyzer are presented in Figure 3.11. The average mean particle sizes of volume-based distributions are shown for each material with the standard error. The PSDs of all sample ranges from 1 μm – 100 μm. The PSD of sample C scattered in a relatively narrow range with overall smaller particle size. Sample B is the coarsest.

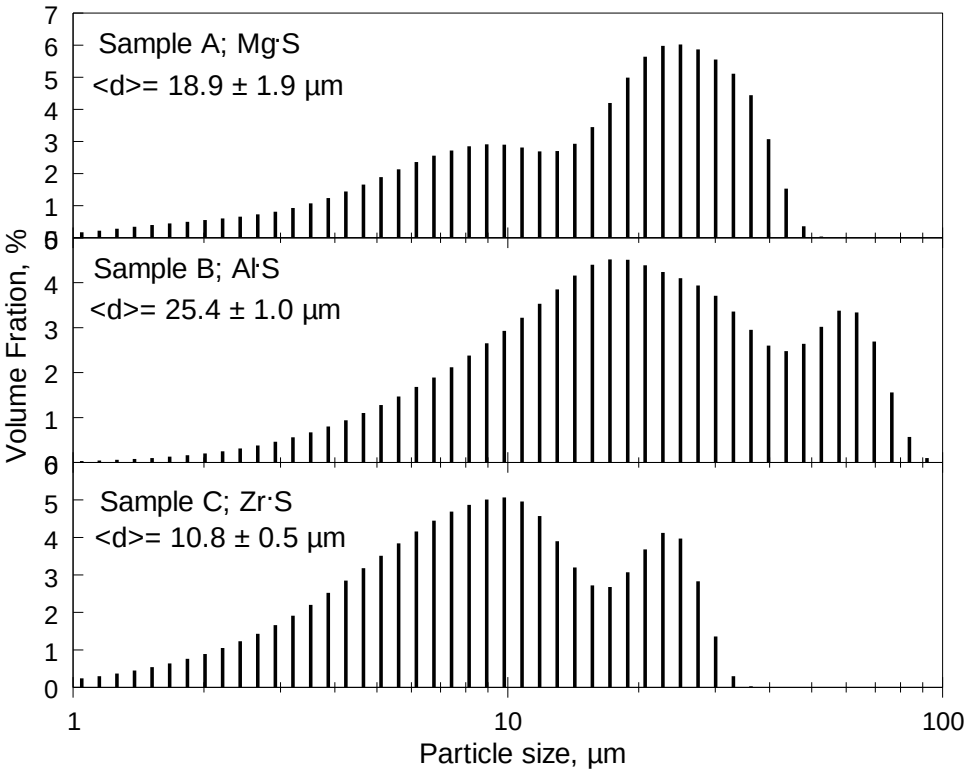

Figure 3.11 Particle size distribution for as milled powders of sample A, B and C measured by the laser scattering with a Coulter particle analyzer.

3.3.2 Phase Composition

XRD patterns for all prepared powders are shown in Figure 3.12. For sample A, in addition to the peaks of elemental magnesium and sulfur, two strong peaks (50° and 62°) of MgS were detected. Thus, sulfide formation in this case was mechanically triggered. However, the reaction was not self-sustained in presence of PCA and only a fraction of magnesium

reacted. XRD patterns for samples B and C only show peaks of elemental metals (Al and Zr, respectively) and peaks of sulfur. No mechanically activated reaction between metal and sulfur occurred for samples B and C.

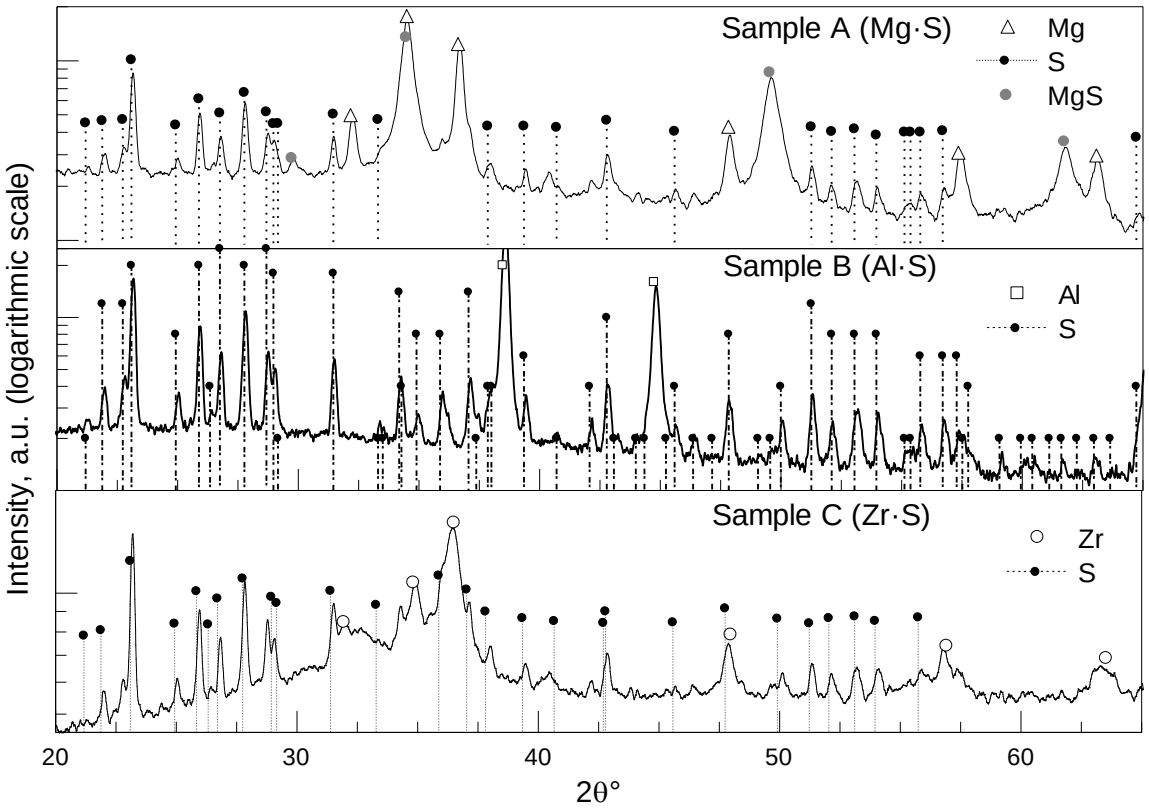

Figure 3.12 X-ray diffraction patterns of as milled powders of sample A, B, and C.

3.3.3 Filament Ignition Experiment

The ignition events were recorded by a high speed camera as illustrated in Figure 3.13. Three image sequences are shown, which are selected as representative runs for each material. All image sequences shown in Figure 3.13 were taken at the heating rate of ~20,000K/s. The first frame in each sequence represents the instant when the initial emission produced by the igniting powder appears. The time, represented by labels in

Figure 3.13, is measured from the moment the wire heating started. Average ignition temperatures measured for different samples at different heating rates are shown in Figure 3.14.

For Mg·S, or sample A, the powder coating the wire ignites nearly instantaneously. Only a very weak light can be seen in the frame taken 36 ms after the start of wire heating. In the next frame, taken at 38 ms, the entire length of the powder coating becomes incandescent. A bright burning cloud is produced at 40 ms and it is growing during the following ca. 4 ms. The combustion event is nearly over at 48 ms, so that the entire duration of the combustion was close to 12 ms.

For Al·S, or sample B, the powder initially is ignited at the edges of the coating. This is caused by temperature gradient along the heated filament. The portion of the filament coated with the powder has effectively higher heat capacity per unit of length, compared to the uncoated filament. Respectively, the temperature of the filament under the coating is slightly lower than that of its uncoated part. This explains initial ignition of the powder at the edges of the coating, where the temperature is higher than closer to the middle of the coating layer. The propagation of the reaction along the coated powder layer takes close to 10 ms. Because the powder does not ignite simultaneously, no bright cloud is produced in this case. The entire duration of the combustion event is close to 28 ms. It should also be noted that the thickness of the powder coating for this powder was likely the smallest. The powder was not well adhering to the wire, unlike samples A and C.

For Zr·S, or sample C, reaction also propagates from the edges of the coating to its center. The initial emission occurs only after 30 ms following the beginning of the experiment, suggesting the lowest ignition temperature, consistently with the data shown

for 20,000 K/s in Figure 3.14. However, the rate of the reaction propagation along the powder coating is lower than for sample B, it takes almost 20 ms for the entire coating to ignite, following its ignition at the edges. The entire reaction lasts for about 42 ms. In the middle of this process, e.g., see the 58-ms frame, large burning fragments are ejected from the powder layer. A diffuse luminous cloud surrounds the burning powder throughout the reaction.

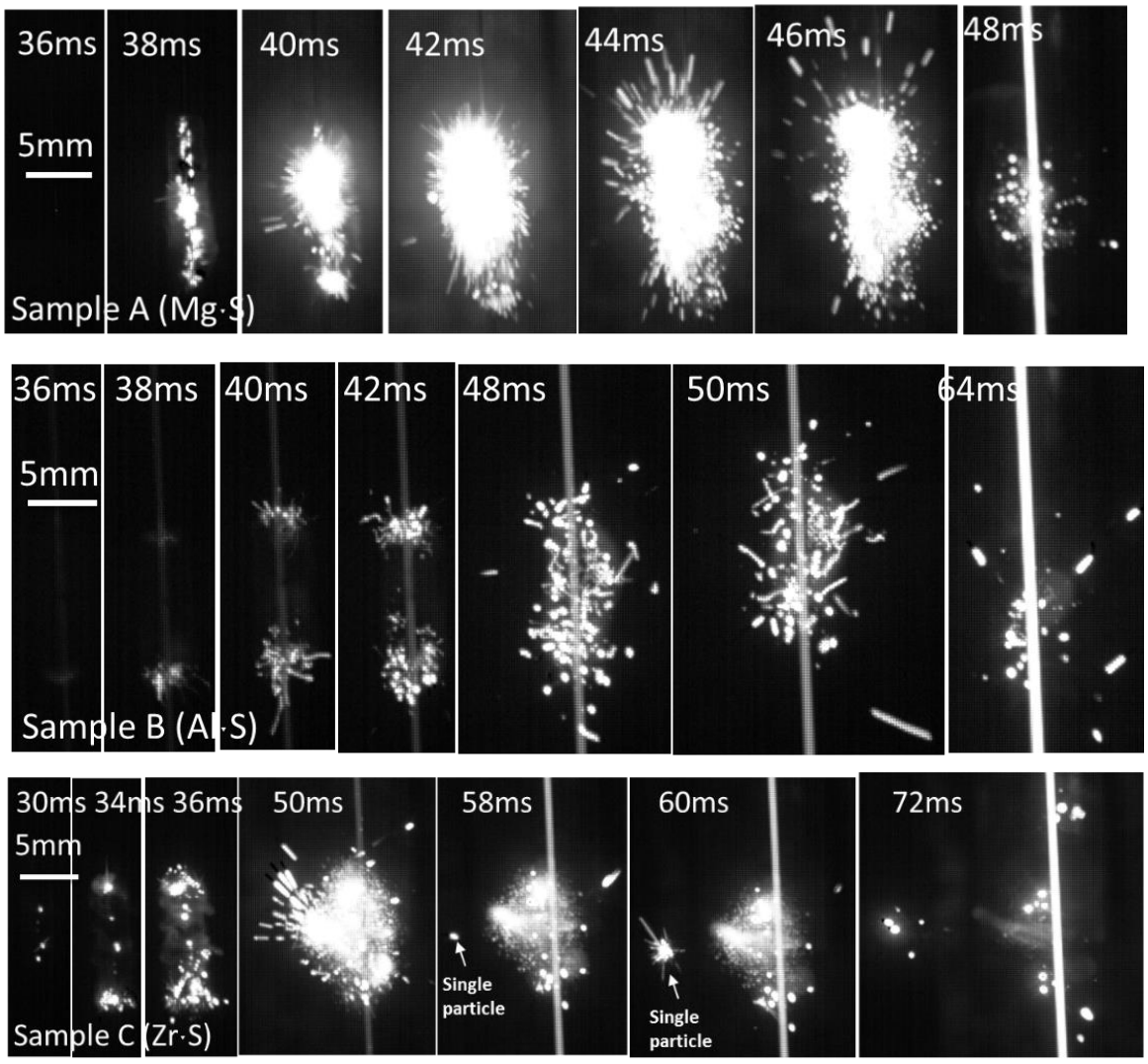

Figure 3.13 Sequences of images captured by high speed camera in the filament ignition experiment for each sample.

Note: The heating rate is 20000 K/s. All images are rotated by 90° for better display. The frame rate is 500 fps and the exposure time for each frame is 2 ms.

The ignition temperature for each sample was measured in the heated filament experiment as a function of the heating rate, as shown in Figure 3.14. Each point represents the average values of the heating rate and ignition temperature with the error bars signifying standard deviations from repeated runs. The ignition temperatures of all samples fall in a range from 750 to 1000 K, which is higher than the boiling point of sulfur, but certainly lower than boiling points of all metals used (see Table 3.2). Consequently, in all cases it is expected that sulfur starts evaporating before ignition, generating a cloud of sulfur above the heated powder. Thus, it is possible that the ignition mechanism of these sulfur containing materials are driven by the initial ignition of vaporizing sulfur. Differences in the ignition temperatures measured at different heating rates for all samples fall within the experimental error bars, and thus are insignificant.

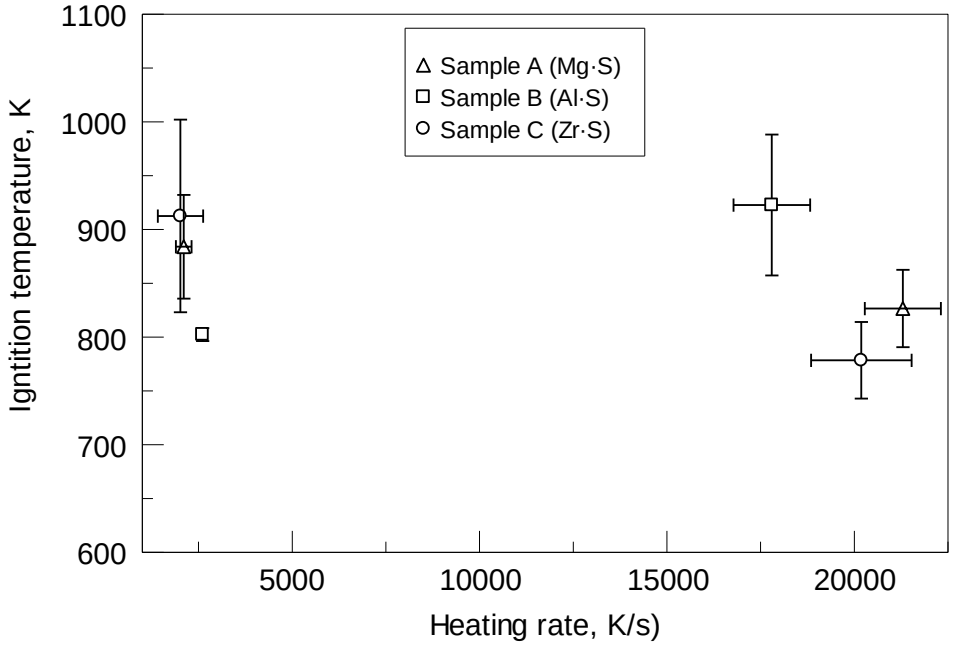

Figure 3.14 Ignition temperatures of sample A, B and C as a function of the heating rate.

Table 3.2 Atmospheric Boiling Points of Elements Used to Prepare Composite Powders

Elements	**Sulfur**	**Magnesium**	**Aluminum**	**Zirconium**
Boiling Point (K)	717	1396	2729	4409

3.3.4 Spark Ignition

Figure 3.15 presents the emission and pressure traces for each sample. The 2000-pF was charged to 12 kV to ignite all samples. The traces shown are as measured, e.g. are not corrected for the amounts of the powders ejected. Note different vertical scales, both for emission signal scaled in V (the detector remained in the same position for all experiments) and for pressure.

The ignition delay based on the optical emission is shortest for sample C. However, this sample produces the weakest emission and pressure pulses among all three samples tested. The pulse durations are approximately 100 ms for all materials. The pressure traces consistently begin with a delay compared to the respective emission signals. The emission peaks for all samples appear to have complex structure. This structure is particularly well visible for sample C, for which emission includes multiple peaks. It is possible that such secondary peaks are caused by formation of agglomerated burning particles, similar to those observed in the videos in Figure 3.13. Normally, the peak in the pressure signal indicates the end of combustion. The emission observed after the pressure peak is commonly interpreted as cooling off combustion products. However, as noted above, emission does not simply decay for sample C even after the pressure peak. If such additional features are caused by few large burning particles, they would not affect the pressure noticeably, but would contribute to the measured optical emission signal.

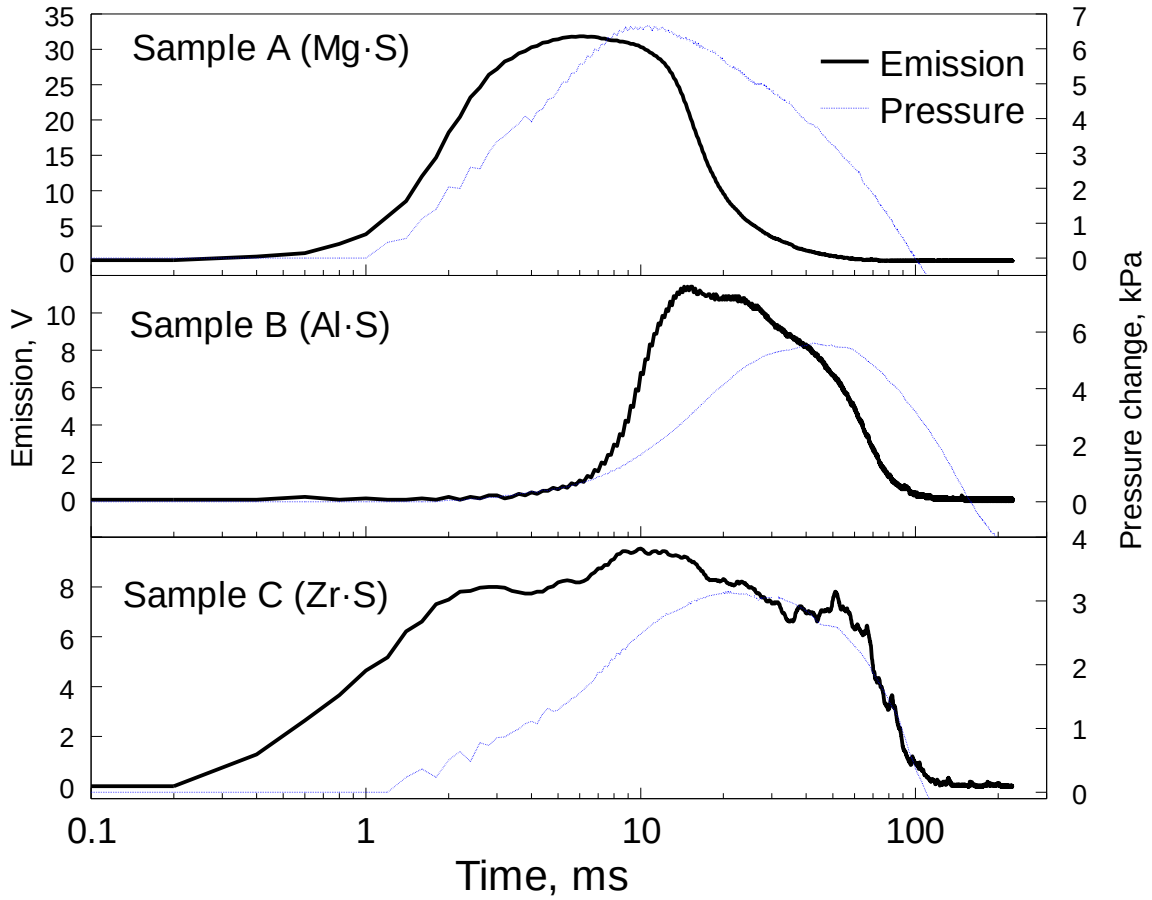

Figure 3.15 Emission traces and pressure signals produced by ESD initiated powders of sample A, B and C.

In Figure 3.16, the maximum pressure and emission are normalized by the weight of ejected powder. Each bar presents the average value for repeated runs with the standard deviation shown as the error bar. Sample B appears to have the highest average normalized pressure as well as the highest average normalized emission. It also appears that the normalized values of pressure and emission signals correlate with each other for all samples.

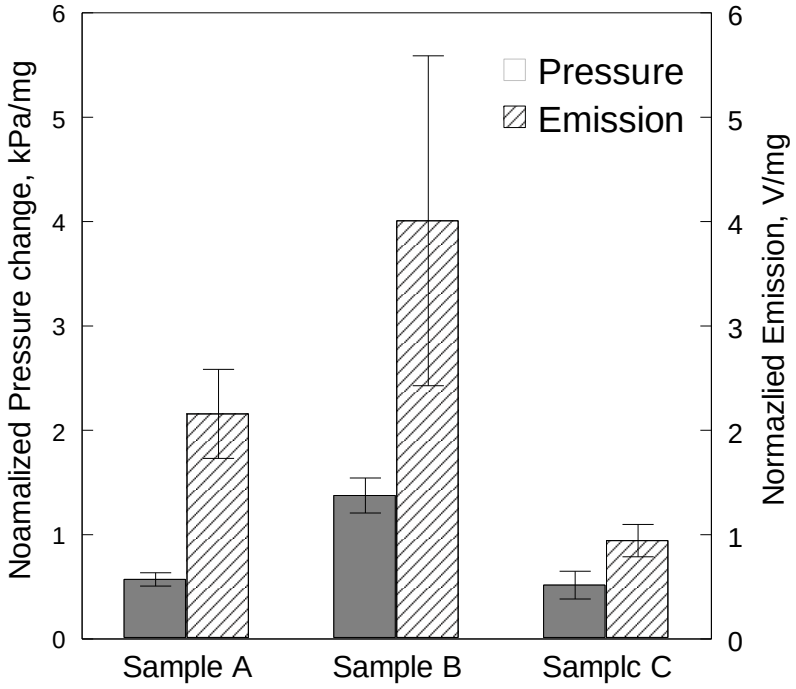

Figure 3.16 Average normalized pressure change and emission produced by ESD initiated powders of sample A, B and C.

Temporal characteristics of the optical emission pulses produced by different materials are summarized in Figure 3.17. Shown are the times corresponding to the emission signal reaching 10 % of its peak value, interpreted as the onset and the burn time, 50 % of its peak value, representing the pulse width, and the peak position. Note that the time is shown in logarithmic scale. The peak position occurs sooner for sample A, while it is most delayed for sample B. Note, however, that the peak is much broader for sample C than for all other materials. The onset of emission occurs for sample C at the shortest times. The overall pulse duration is the shortest for sample A, suggesting the highest overall rate of energy release for this material.

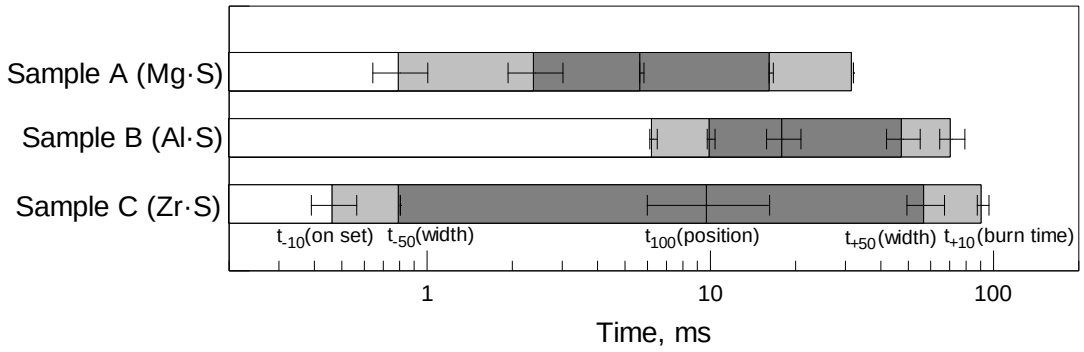

Figure 3.17 Average temporal characteristics of optical emission pulses produced by ESD initiated powders of samples A, B, and C.

To test the sensitivity of each sample to ESD ignition, the spark energy was changed to determine the minimum input energy necessary to ignite the powder. The voltage varied between 3 and 12 kV; the capacitor was changed in a range of 100pF - 2000pF. Experimental results are shown in Figure 3.18. The input energy calculated by varying the combination of voltage and capacitor are shown as X-axis. For samples B and C, the emission intensity increases when higher ESD energy is used to ignite the powder. It is likely because more powder was ignited with the higher spark energy. On the other hand, the peak emission of sample A was quite high for all spark energies. No clear trend for that material was observed. Sample A ignited at the lowest energies used in the present experiments, indicating that it is most sensitive to the ESD spark.

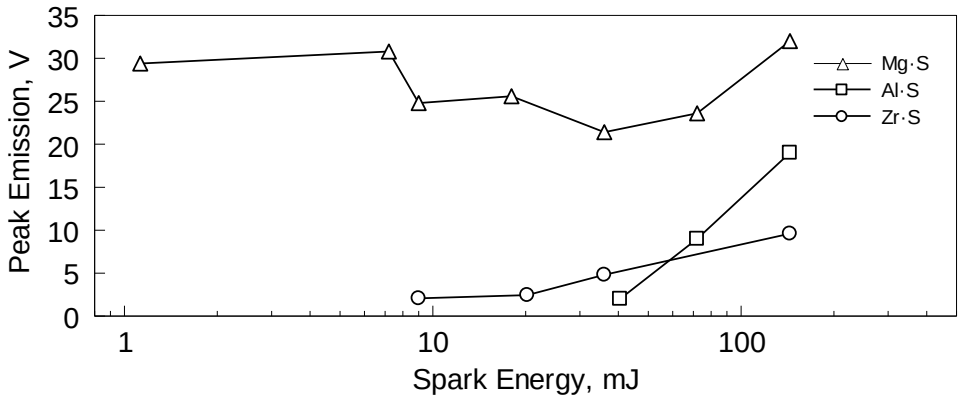

Figure 3.18 The peak emission of the each ignited sample powder in ESD test as a function of spark energy.

3.3.5 Aerosol Combustion

Examples of pressure traces obtained from CVE experiment are shown in Figure 3.19. Time zero corresponds to the time when the thermite igniter placed in the center of the combustion vessel is initiated. It appears that sample A ignited faster than samples B and C. The shortest ignition delay of sample A indicates its higher reactivity compared to other two samples. Among three samples, sample C has the lowest maximum pressure and longest ignition delay.

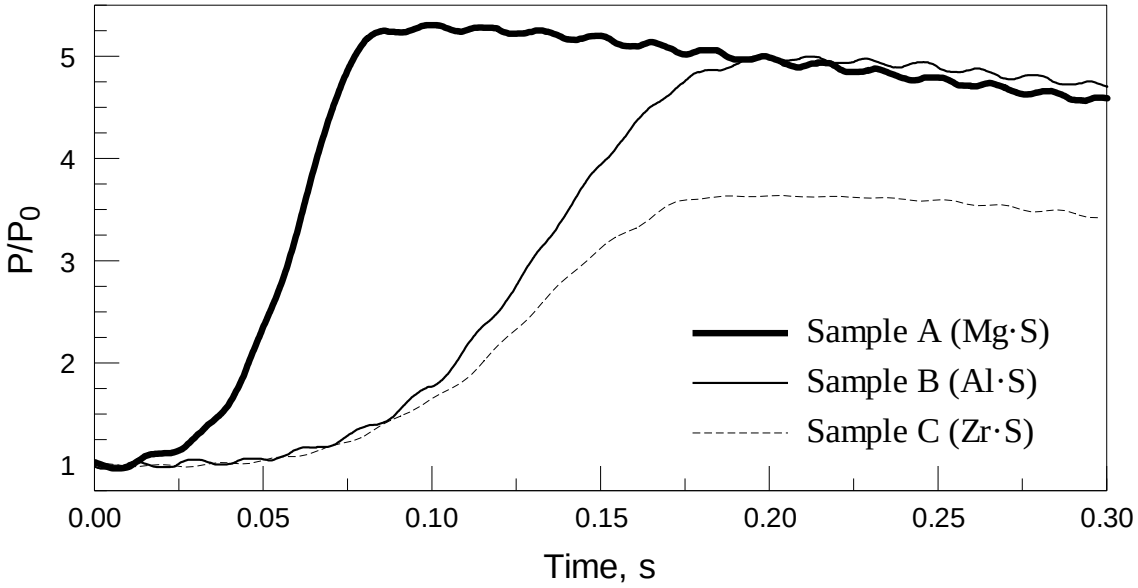

Figure 3.19 Normalized pressure traces of ignited powders of sample A, B, and C measured in CVE test.

A summary of the CVE test performance for all samples is given in Figure 3.20. The average values of the maximum pressure, P_{max}, and the maximum rate of pressure rise, $(dP/dt)_{max}$, both normalized by the initial pressure in the vessel, P_0, are presented with the standard error bars for samples A and B. Note that the experiments for sample C could not be repeated because in most runs, this material ignited while entering the combustion

vessel, i.e., before the igniter was initiated. The ignition was triggered mechanically, when the powder passed through the dispersion nozzle. Because in these cases, the gas flow in the vessel was much more turbulent than in the other experiments, recorded pressure pulses cannot be meaningfully compared to those recorded in other experiments.

Assessments of the combustion efficiency for different samples were obtained by comparing the experimentally determined pressure ratio P_{max}/P_0 with those predicted by the thermodynamic equilibrium calculations using NASA CEA code [21]. A constant volume configuration was selected for the calculations. The actual mass of the powder load and the volume of the vessel were accounted for. The results indicate that sample A generates the highest pressure and has the highest combustion efficiency among all samples. This correlates with its highest combustion rate, or greatest value of $[d(P/P_0)/dt]_{max}$.

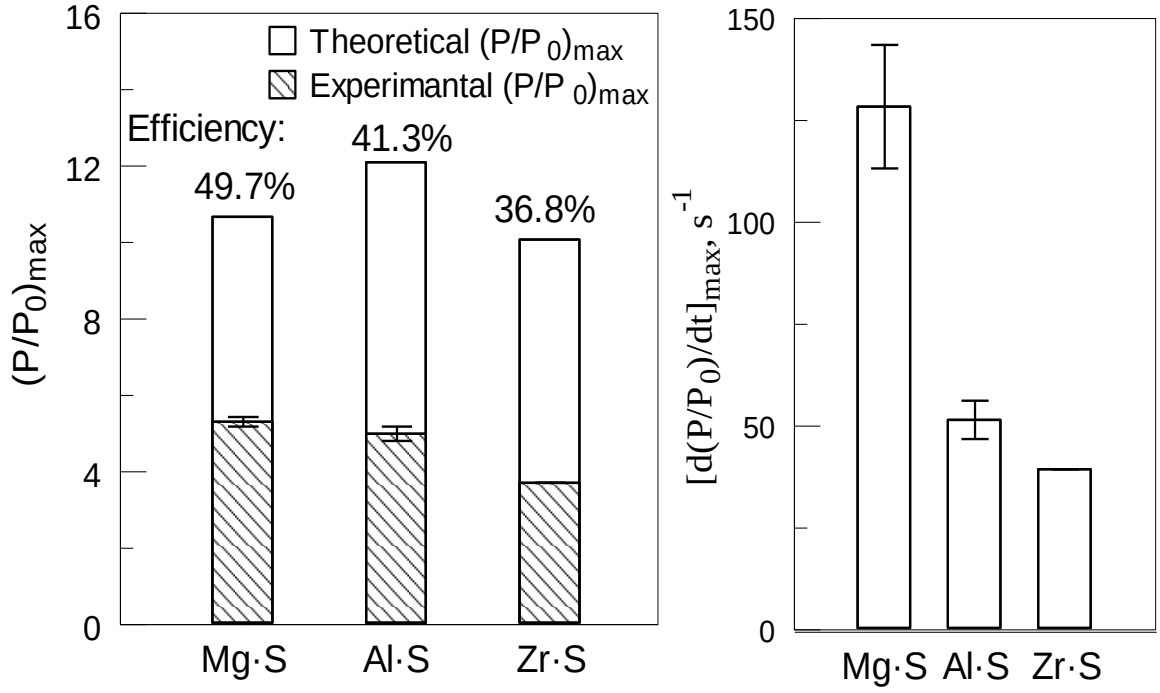

Figure 3.20 Summary of CVE results.

Condensed combustion products were collected for all samples and characterized by XRD. Figure 3.21 presents the XRD patterns of the combustion products for different materials. For sample A, no unreacted magnesium is detected. The products contain primarily a mixture of MgS and MgO. Weak peaks of sulfur are also detectable.

For samples B and C, apparent peaks of Al and Zr were detected suggesting an incomplete reaction. In addition to metal oxides and sulfur, for sample C weak patterns suggesting formation of complex zirconium sulfides, such as Zr_9S_2, are observed. For sample C, in particular, the mixing between Zr and S was not as good as for other materials. Thus, it is expected that optimizing milling conditions used to prepare such material may improve its combustion performance noticeably.

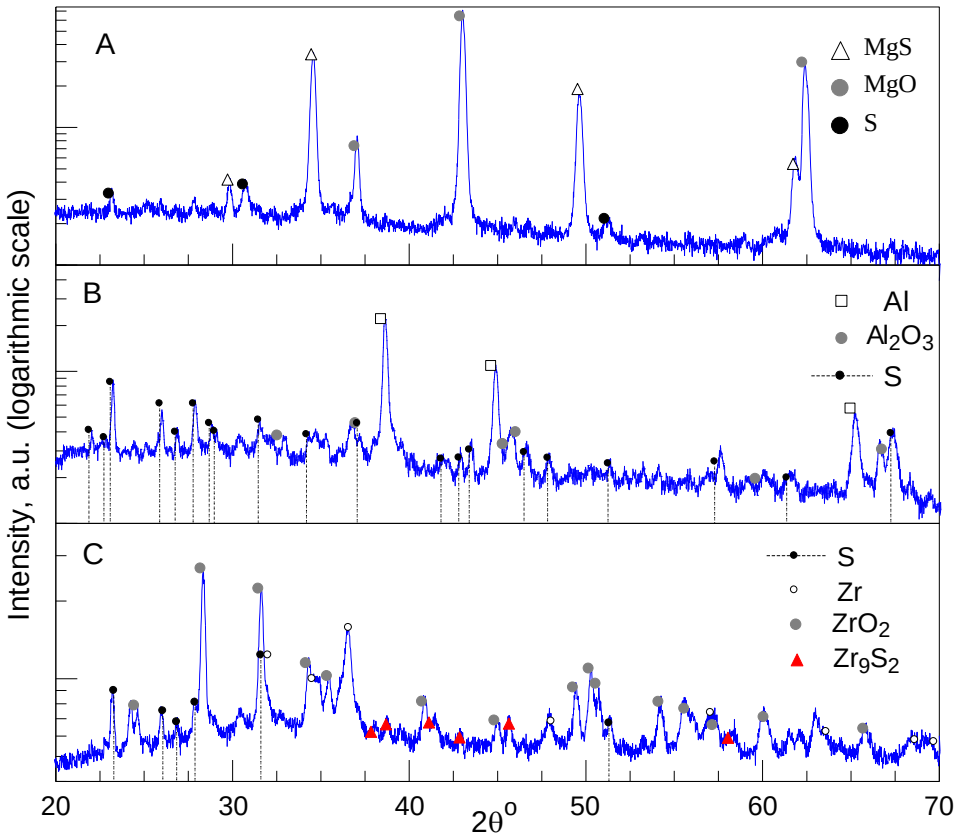

Figure 3.21 XRD patterns of CVE combustion products.

CHAPTER 4

DISCUSSION

In this section, the relations between particle sizes, ignition properties and combustion performance characterized by different methods will be discussed. Figure 4.1 presents the highest rate of pressure rise measured in the CVE experiment as a function of the ignition temperature. The data are shown for both heating rates used in the heated filament ignition experiments. No apparent trend is observed for either heating rate, considering all three materials. Thus suggests that the ignition temperature measured in the heated filament ignition tests was not the parameter governing the flame propagation in the CVE experiments. Flame propagation is expected to be affected by heat transfer in the aerosolized cloud, which leads to heating and ignition of individual particles.

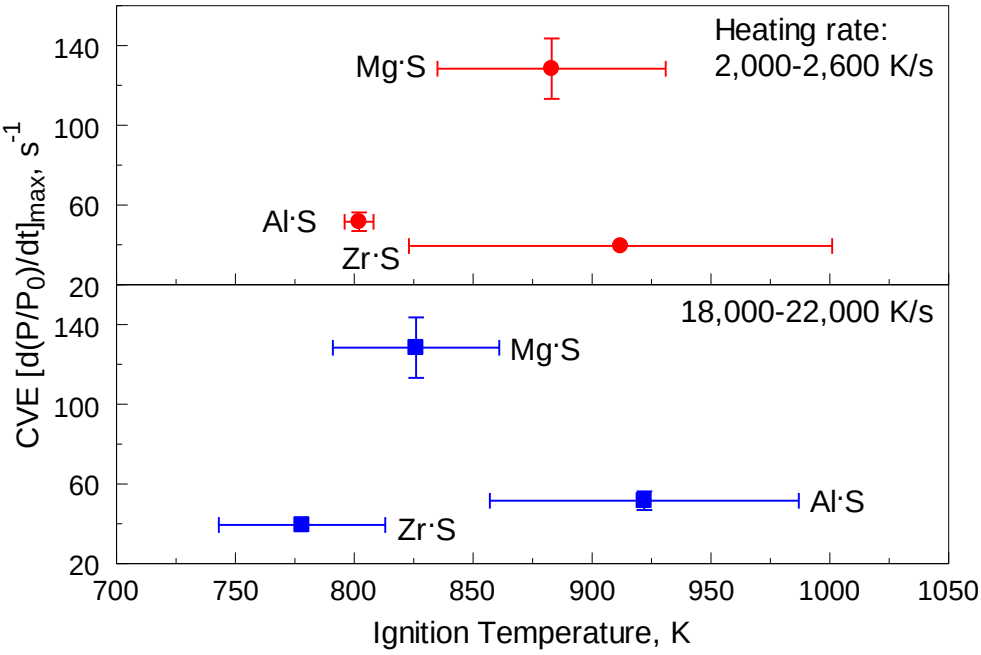

Figure 4.1. The maximum rates of pressure rise measured in the CVE tests as a function of ignition temperatures.

A correlation between particle sizes and the rate of pressure rise observed in the CVE experiments is shown in Figure 4.2. Once again, there is no consistent trend for all three materials. However, considering only Mg·S and Al·S, the larger particle size correlates with the lower rate of flame propagation, or smaller rate of pressure rise.

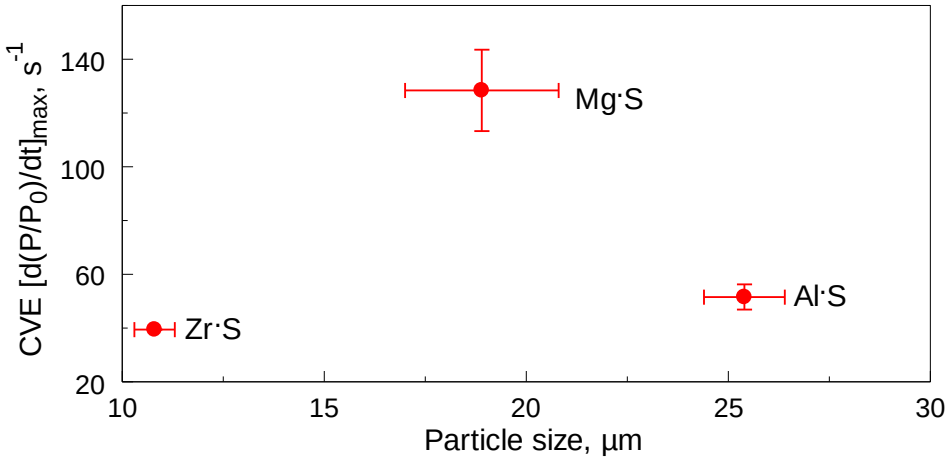

Figure 4.2 The maximum rates of pressure rise measured in the CVE tests as a function of the average particle size.

In Figure 4.3, a correlation of ignition delay obtained in the ESD ignition test and ignition temperature measured in heated filament experiment is shown. Two opposite trends are observed for the ignition temperatures measured at different heating rates. The trend for the higher heating rate is sensible: higher ignition temperatures lead to greater ignition delays. The opposite trend observed for the ignition temperatures obtained at a low heating rate suggests that the ignition mechanism changes as a function of the heating rate.

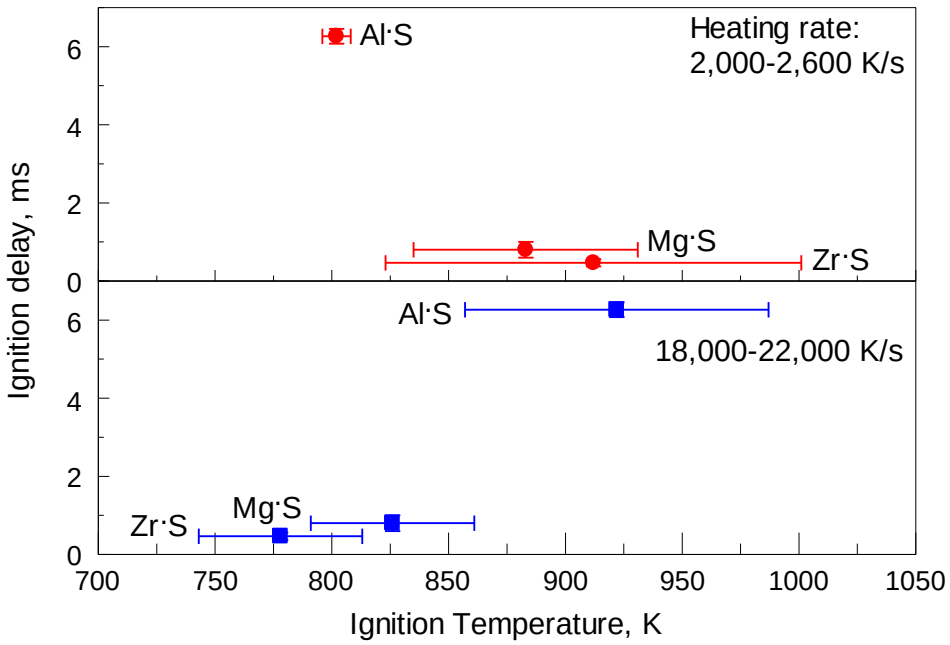

Figure 4.3 Ignition delays measured in the ESD tests as a function of the ignition temperatures.

Figure 4.4 shows a correlation between average particle sizes and ignition delay measured in the ESD tests. There is a correlation suggesting that larger particles ignite later. This correlation is sensible.

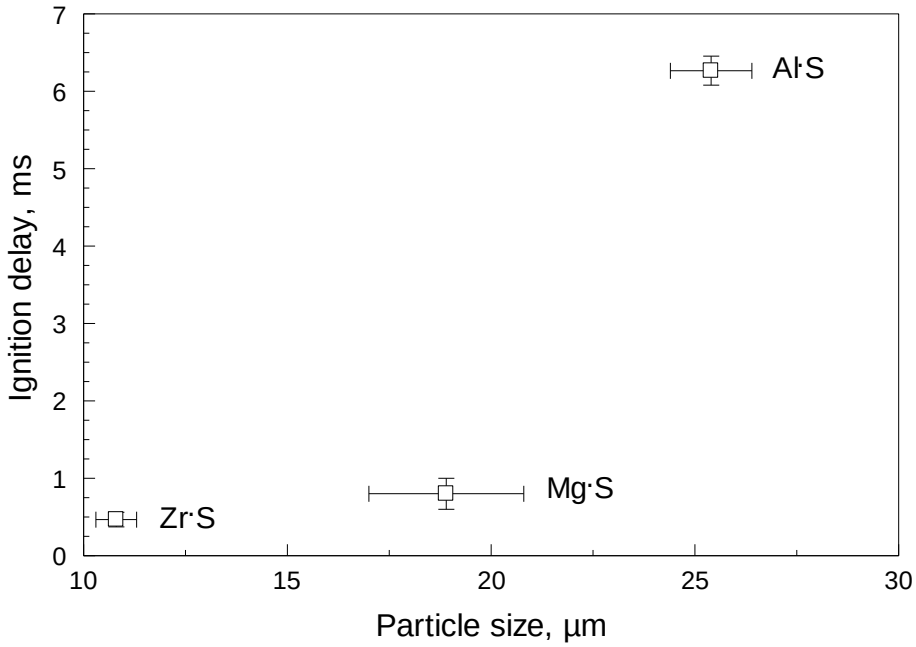

Figure 4.4 Ignition delays measured in the ESD tests as a function of the average particle sizes.

Figure 4.5 exhibits the effect of ignition temperature on normalized pressure measured in the ESD test. Once again, opposite trends are observed for the ignition temperatures measured at different heating rates. The correlation for the temperature corresponding to the higher heating rates suggests that a greater pressure is produced for the samples ignited at a higher temperature. Because the pressure in the ESD ignition tests is generated by the burning particle cloud, as opposed to individual particles ignited directly by the spark, this correlation may be reasonable. A higher ignition temperature may suggest that fewer particles were ignited directly by the spark; instead more particles ejected by the shock associated with the spark were later ignited in the cloud. This trend might deserve further analysis in the future work.

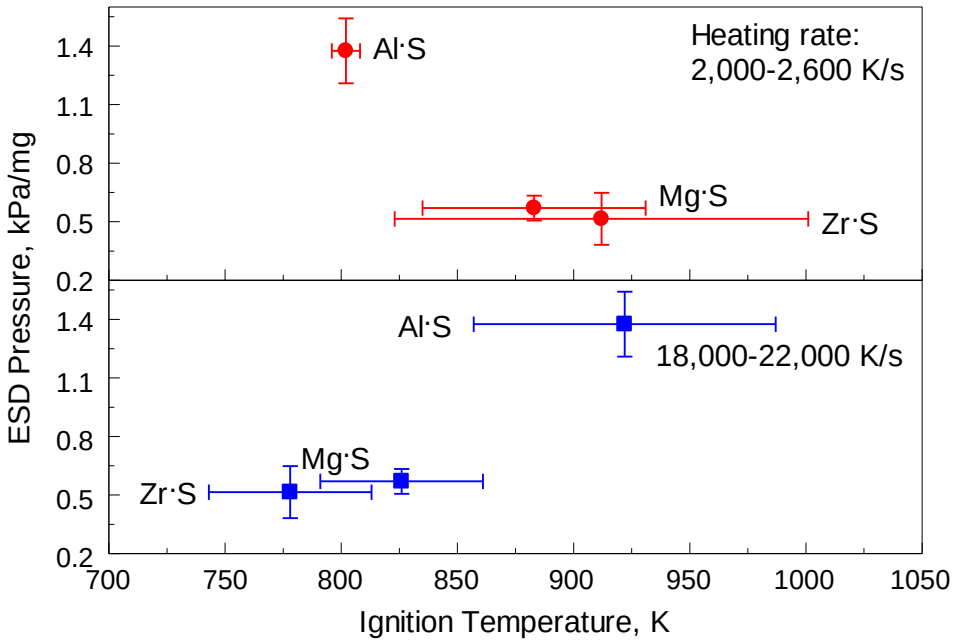

Figure 4.5 Maximum normalized pressure of each sample measured in ESD test as a function of ignition temperatures.

Figure 4.6 considers a relation between burn times of ignited powder and respective powder mean particle size. Although the particle size of sample A is not the smallest among

all sample, it still burns out in shortest time period. Because the burn time is characterizing the cloud combustion rather than single particle combustion, it is affected by both particle size as well as by the size of the produced and ignited cloud. Thus, the correlation shown in Figure 4.6 may mean either a very high reactivity of Mg·S composite (sample A), or a small size of the cloud it produces.

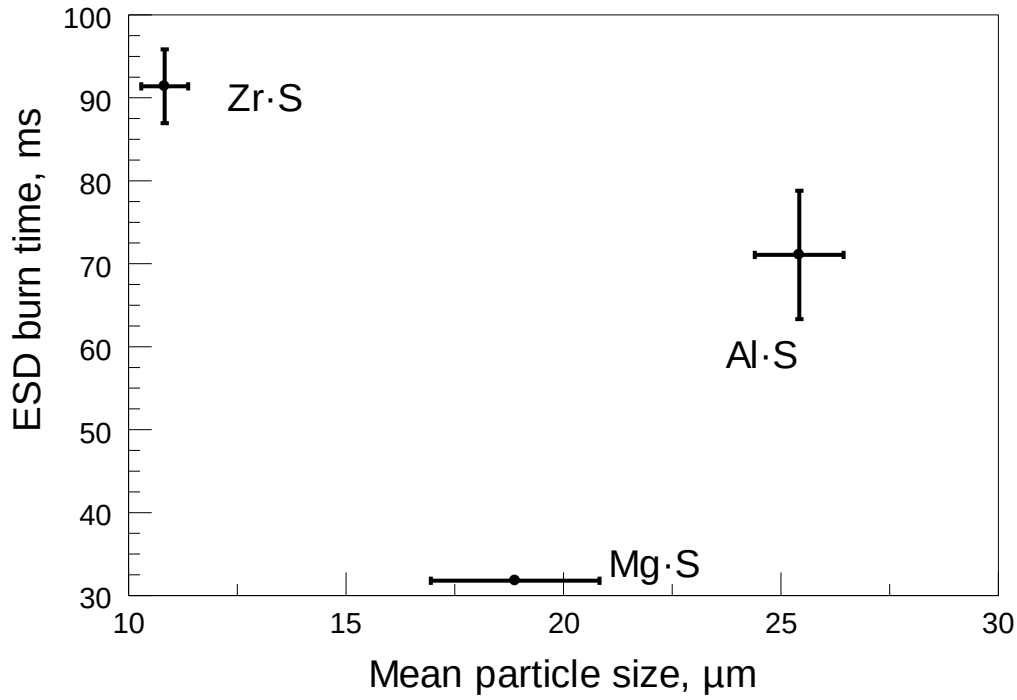

Figure 4.6 Burn time of each sample measured in ESD test as a function of mean particle size.

The correlation between the burn time measured in the ESD test and the rate of pressure rise in the CVE experiment is illustrated in Figure 4.7. It appears that samples with shorter burn time exhibit higher rates of pressure rise. Both parameters characterize the burn rate, and thus the correlation is very reasonable. The correlation shown in Figure 4.7 is useful for future analyses of the powder burn rates; it enables one to predict the powder performance in the CVE configuration using data from a much smaller scale ESD ignition

test. We speculate that the combustion rate of aerosolized powder is affected by the reactivity of powder, which is represented by the burn time measured in ESD experiment.

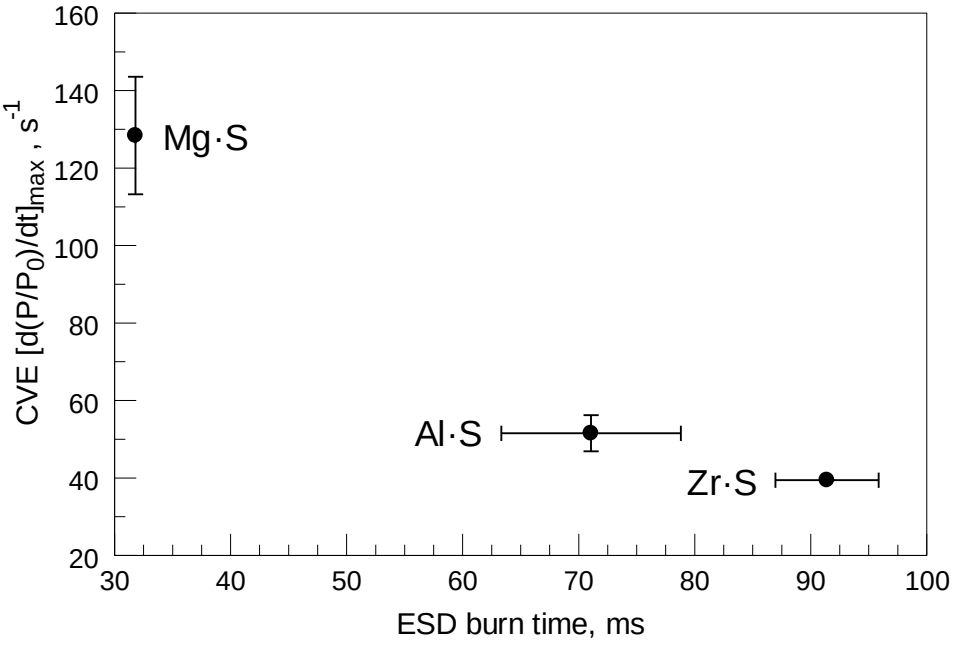

Figure 4.7 Maximum rate of pressure rise measured in CVE test as a function of burn time measured in ESD test.

As shown in Figure 4.8, the mutual influence of measured parameters in CVE and ESD were discussed. There is no clear correlation between normalized pressure of each sample measured in ESD and normalized pressure measured in CVE. It should be noticed that pressure measured in the CVE test was normalized by the initial pressure, e.g. 1 atmosphere; pressure acquired in ESD test was normalized by weight of ejected powder. However, interestingly, samples producing greater absolute pressure in the ESD tests also have higher normalized CVE pressures. In both cases, the pressure is affected by how well the powder is aerosolized. This correlation suggests that this effect, associated with the degree of agglomeration of lifted particles, may be important in affecting combustion of the materials in both CVE and ESD experiments.

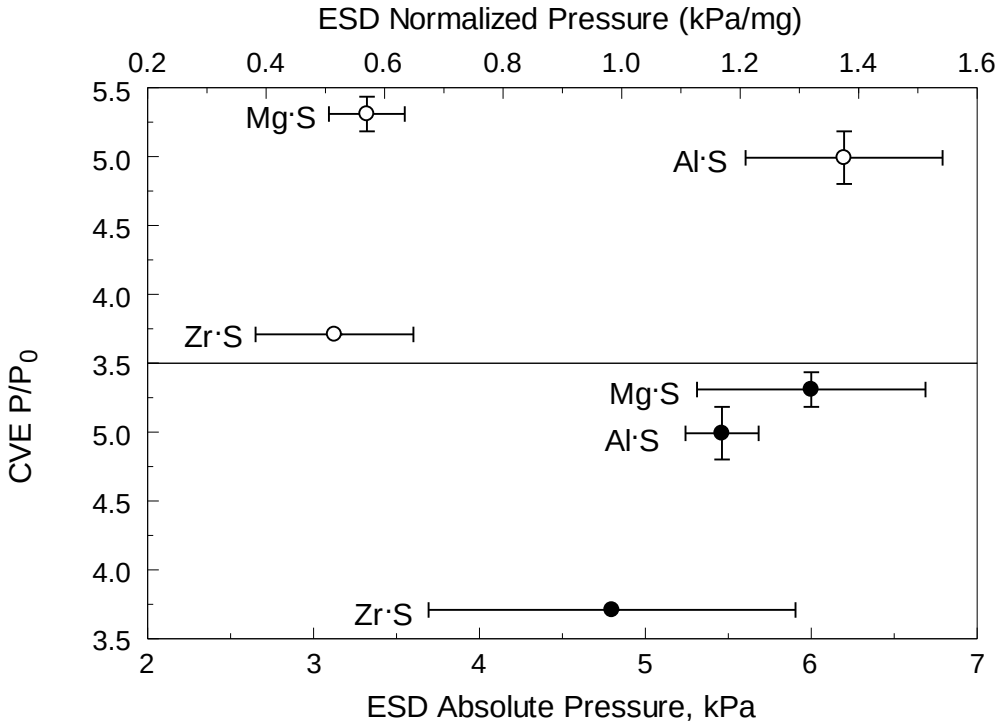

Figure 4.8 Maximum normalized pressure measured in CVE test as a function of both normalized pressure and absolute pressure measured in ESD test.

CHAPTER 5

CONLUSION

Mechanical milling can be used to prepare reactive composite metal-sulfur powders using different metals. Specifically, reactive materials were prepared with Al, Mg, and Zr mixed with sulfur. For Mg·S composite, reaction between Mg and S could not be completely avoided and the prepared material included a fraction of MgS. No reaction occurred for Al and Zr based composites, although the milling conditions used to prepare these materials were not optimized to reduce the scale of mixing between components. All prepared materials ignited in the relatively narrow range of temperatures of 750 – 1000 K. All materials could be successfully ignited by an electrostatic discharge. The ignition delays correlated with the particle sizes for different materials. The pressures and emission intensities generated by the ESD-ignited powders correlated with each other, suggesting that either measurement provides a gauge for the combustion performance. Combustion tests were also performed in the constant volume explosion setup. In most tests with Zr·S powder, ignition was mechanically triggered when the powder was introduced in the chamber. However, successful experiments were performed with both Al and Mg-based composites. The combustion pressures were relatively low, which is not unusual for these tests. Comparatively, the highest absolute pressure and the highest combustion efficiency were observed for Mg·S powder. Similarly, this powder exhibited the highest rate of pressure rise in these experiments. The rates of pressure rise measured for all materials in the CVE tests correlate with the burn times of the same materials ignited by ESD,

suggesting that both experimental methods can be used to assess the reaction rates of the prepared materials.

REFERENCES

[1] X. Zhu, M. Schoenitz, E.L. Dreizin, Aluminum powder oxidation in CO2 and mixed CO2/O 2 environments, *Journal of Physical Chemistry C* 113 (2009) 6768-6773.

[2] K.T. Sullivan, C. Wu, N.W. Piekiel, K. Gaskell, M.R. Zachariah, Synthesis and reactivity of nano-Ag2O as an oxidizer for energetic systems yielding antimicrobial products, *Combustion and Flame* 160 (2013) 438-446.

[3] B.R. Clark, M.L. Pantoya, The aluminium and iodine pentoxide reaction for the destruction of spore forming bacteria, *Physical chemistry chemical physics* 12 (2010) 12653-12657.

[4] S. Zhang, C. Badiola, M. Schoenitz, E.L. Dreizin, Oxidation, ignition, and combustion of Al·I 2 composite powders, *Combustion and Flame* 159 (2012) 1980-1986.

[5] S. Zhang, M. Schoenitz, E.L. Dreizin, Iodine release, oxidation, and ignition of mechanically alloyed Al-I composites, *Journal of Physical Chemistry C* 114 (2010) 19653-19659.

[6] A. Abraham, S. Zhang, Y. Aly, M. Schoenitz, E.L. Dreizin, Aluminum-iodoform composite reactive material, *Advanced Engineering Materials* (2014).

[7] A. Abraham, J. Obamedo, M. Schoenitz, E.L. Dreizin, Effect of composition on properties of reactive Al·B·I2 powders prepared by mechanical milling, *Journal of Physics and Chemistry of Solids* 83 (2015) 1-7.

[8] S. Wang, A.L. Corcoran, V. Leybova, E.L. Dreizin, Metal-Based Iodine Bearing Materials Prepared by Mechanical Milling, MRS Online Proceedings Library 1758 (2015) null-null.

[9] V. Sambhy, M.M. MacBride, B.R. Peterson, A. Sen, Silver bromide nanoparticle/polymer composites: Dual action tunable antimicrobial materials, *Journal of the American Chemical Society* 128 (2006) 9798-9808.

[10] J. Kalman, N.G. Glumac, H. Krier, Experimental Study of Constant Volume Sulfur Dust Explosions, *Journal of Combustion* 2015 (2015) 1-11.

[11] S. Goroshin, A. Miera, D.L. Frost, J.H.S. Lee, Metal-sulfur combustion, *Symposium (International) on Combustion* 26 (1996) 1883-1889.

[12] E.L. Dreizin, M. Schoenitz, Nano-composite energetic powders prepared by arrested reactive milling, US Patent 7,524,355 2009.

[13] M. Schoenitz, T.S. Ward, E.L. Dreizin, Fully dense nano-composite energetic powders prepared by arrested reactive milling, *Proceedings of the Combustion Institute* 30 (2005) 2071-2078.

[14] S.M. Umbrajkar, S. Seshadri, M. Schoenitz, V.K. Hoffmann, E.L. Dreizin, Aluminum-rich Al-MoO3 nanocomposite powders prepared by arrested reactive milling, *Journal of Propulsion and Power* 24 (2008) 192-198.

[15] A. Abraham, Z. Zhong, R. Liu, S.A. Grinshpun, M. Yermakov, R. Indugula, M. Schoenitz, E.L. Dreizin, Preparation, ignition and combustion of Mg·S reactive nanocomposites, *Combustion Science and Technology* In Press (2016).

[16] Y.L. Shoshin, M.A. Trunov, X. Zhu, M. Schoenitz, E.L. Dreizin, Ignition of aluminum-rich Al-Ti mechanical alloys in air, *Combustion and Flame* 144 (2006) 688-697.

[17] T.S. Ward, M.A. Trunov, M. Schoenitz, E.L. Dreizin, Experimental methodology and heat transfer model for identification of ignition kinetics of powdered fuels, *International Journal of Heat and Mass Transfer* 49 (2006) 4943-4954.

[18] R.A. Williams, E. Beloni, E.L. Dreizin, Ignition of metal powder layers of different thickness by electrostatic discharge, *Journal of Propulsion and Power* 28 (2012) 132-139.

[19] R.A. Williams, J.V. Patel, E.L. Dreizin, Ignition of fully dense nanocomposite thermite powders by an electric spark, *Journal of Propulsion and Power* 30 (2014) 765-774.

[20] D. Stamatis, Z. Jiang, V.K. Hoffmann, M. Schoenitz, E.L. Dreizin, Fully dense, aluminum-rich Al-CuO nanocomposite powders for energetic formulations, *Combustion Science and Technology* 181 (2009) 97-116.

[21] B.J. McBride, S. Gordon, Computer Program for Calculation of Complex Chemical Equilibrium Compositions and Applications II. Users Manual and Program Description., NASA RP 1311, 1996.